MASSACHUSETTS INSTITUTE OF TECHNOLOGY

HYDRODYNAMICS LABORATORY

DEPARTMENT OF CIVIL AND SANITARY ENGINEERING

TECHNICAL REPORT NO. 35

MEASUREMENT AND ANALYSIS OF TURBULENT FLOW OF WOOD PULP FIBER SUSPENSIONS

by

J. W. DAILY, G. BUGLIARELLO AND W. W. TROUTMAN

SEPTEMBER, 1959

PREPARED UNDER CONTRACT
WITH THE
TECHNICAL ASSOCIATION
OF THE
PULP AND PAPER INDUSTRY

HYDRODYNAMICS LABORATORY

Department of Civil and Sanitary Engineering

Massachusetts Institute of Technology

MEASUREMENT AND ANALYSIS OF TURBULENT FLOW OF WOOD PULP FIBER SUSPENSIONS

by

J. W. Daily, G. Bugliarello and W. W. Troutman

September, 1959

Technical Report No. 35

Prepared Under Contract

with the

Technical Association of the Pulp and Paper Industry

ACKNOWLEDGEMENT

This investigation was conducted in the Hydrodynamics Laboratory of the Massachusetts Institute of Technology under the sponsorship of the Technical Association of the Pulp and Paper Industry as TAPPI Research Project 147.

The investigation was conducted under the supervision of Professors James W. Daily and Arthur T. Ippen. The experimental work was performed by Mr. W. W. Troutman and Dr. George Bugliarello, both of whom have been associated with the TAPPI sponsored research program from its inception.

ABSTRACT

In a previous report techniques were described for measuring turbulence and velocity profiles in turbulent shear flows of water and dilute fiber suspensions, and some preliminary results presented. The present report describes subsequent experience with the techniques, and the results of their application to an extended range of flow velocities and an additional wood pulp suspension. The report has two areas of emphasis. The first has to do with some basic facts about turbulence, together with relevant theoretical relations among variables and their implications as regards problems of measurement and analysis. The second relates to the specific measurements and their significance as regards flowing fiber suspensions.

The results confirm and extend the previous conclusions regarding the mechanism of turbulence and the momentum transfer process in dilute fiber suspensions. In particular, the significance of the combined roles of turbulence and fiber entanglement in diffusion and mixing is examined in detail. The necessity of isolating these roles is discussed and recommendations presented. The procedures employed for data measurement and analysis of the statistically turbulent flow are analyzed and recommendations made.

CONTENTS

TABLES

FIGURES

NOTATIONS AND DEFINITIONS

Autocorrelation function. A function defined by Eq. [1]

Autocorrelogram. A function defined by Eq. [2]

c = concentration

D = pipe diameter

f = friction factor $= \dfrac{\Delta P}{\gamma \dfrac{L}{D} \dfrac{V^2}{2g}}$

$F(n)$ = fraction of kinetic energy per unit mass of the x-component of the turbulent fluctuations, referred to the maximum energy density occuring in the entire spectrum. Defined by Eq. [4]

$F_1(n)$ = fraction of total kinetic energy per unit mass of the x-component of the turbulent fluctuations, and per unit bandwidth. Defined by Eq. [6]

g = acceleration of gravity

H = instantaneous dynamic head acting on impact tube (Eq. [12])

ΔH = head loss

k = von Karman constant (Eq. [19])

k_c, k = (in Fig. 17) hypothetical variations of k with concentration and Reynolds number respectively

ℓ = fiber length

L = length of pipe over which a given pressure drop ΔP occurs

n = frequency, cps $(=\omega/2\pi)$

Δn = frequency interval (bandwidth)

ΔP = pressure drop

p' = local turbulent pressure fluctuation

$R(\tau)$ = autocorrelation function. Defined by Eq. [1]

$R(\tau_1 T)$ = autocorrelogram. Defined by Eq. [2]

$\mathcal{R}$ = Reynolds number $= \dfrac{VD}{\nu}$

t = time

T = a time interval; specifically, length of autocorrelogram

$\bar{u}$, u = local mean velocity in the x-direction

u' = x-component of turbulent velocity fluctuation

U, U_{max} = max velocity in the x-direction at centerline of pipe

v' = y-component of turbulent velocity fluctuation

V = average bulk velocity (= discharge/area of cross-section)

x, y, z	=	orthogonal coordinate axes; x is in the direction of the mean flow (parallel to pipe axis); y often denotes distance from pipe wall
Y_A	=	ordinate of autocorrelation function or of autocorrelogram, at $\tau = 0$. Defined respectively by Eq. [1a] and [2a]
γ	=	specific weight
ϵ	=	local momentum transfer coefficient. Defined by Eq. [15]
ν	=	Kinematic viscosity of water
τ	=	local shear stress; also, in autocorrelation measurements, delay time (see e.g. Eq. [1])
τ_w	=	wall shear stress
$\Phi(n)$	=	energy spectrum function: average kinetic energy per unit mass at a point in the flow, contained in a given frequency bandwidth Δn, divided by the bandwidth
ω	=	angular frequency ($=2\pi n$)
ω_o	=	frequency of periodicities in autocorrelation record
Ω	=	rotating speed of pump
Ω_b	=	frequency of pump rotor vanes passing the volute tongue (cutwater)

I. INTRODUCTION

In a previous report [Ref. (29)], techniques were described for measuring turbulence and velocity profiles in turbulent shear flows of water and dilute fiber suspensions, and some preliminary results presented. The present report describes subsequent experience with the techniques and the results of their application to an extended range of flow velocities and an additional wood pulp suspension.

For the case of turbulence, the essentially statistical nature of the phenomenon introduces special problems into both the data measurement and data analysis and interpretation. Because of this, the report has two areas of emphasis. The first has to do with some basic facts about turbulence, together with relavent theoretical relations among variables and their implications as regards problems of measurement and analysis in the present investigation. The second is the discussion of the specific measurements of turbulence and velocity profiles and their significance as regards flowing fiber suspensions.

II. SOME ASPECTS OF TURBULENCE AND METHODS OF THEORETICAL AND EXPERIMENTAL ANALYSIS

1. General

Turbulence is characterized by irregular unsteady fluctuating motions of small fluid masses within a larger field of flowing fluid. These motions are random to various degrees depending on the circumstances leading to the turbulence. As a random process, the precise form of motion of a turbulent field cannot be described or predicted. However, it is possible to characterize different states of turbulence through its statistical properties. By averaging in different desired ways the various properties from a turbulence record, meaningful statistical quantities are obtained.

In general we can think of two types of turbulent behavior and two corresponding types of averaging. In one, the actual motion at some point in a field is a fluctuation about a certain mean state. Averages over a period of time tend to assume definite values if the time interval is long enough. In the second, the motion appears to have the same character over a definite part of the field. Then averaging a quantity over the particular domain at some instant of time gives a definite value. Statistically the field appears to be homogeneous, and, following Bendat [Ref. (18)], the turbulence is said to be a stationary random process. In principle a homogeneous turbulent field may be stationary with respect to time also so that time averages may replace space averages as is discussed in more detail later. If this can be assumed experimental simplification occurs automatically.

For homogeneous turbulence there is no variation in mean velocity in any direction and no net shear stress transmitted across the turbulent field. However, in many practical cases where shear stresses exist, there may be some degree of homogeneity. The quasi-steady turbulent shear flow in a long cylindrical pipe or rectangular channel is a combination of the two kinds of behavior just mentioned. The statistical properties at each point in the pipe are independent of time, and on every straight line parallel to the axis are independent of distance. Therefore, on any radius turbulence records should have the characteristics of a stationary random function of both space (distance) and time, and some of the concepts applicable to the analysis of stationary random processes will be useful in the study of such a shear flow.

There is a limitation to the usefulness of statistical methods in arriving at a clear physical understanding of turbulence. It is true that statistical concepts introduced by the mathematical studies of isotropic and homogeneous flows are exerting an ever widening and clarifying influence on our interpretation of the turbulent process in shear flows. However, when we seek to correlate the characteristics of the turbulent field and the mean flow velocities of these shear flows, we must still rely heavily on elementary or phenomenological models (e.g. mixing length, momentum transfer coefficients, Reynolds shear stresses, etc.).

The recourse to elementary models becomes even more necessary when we

first start investigating complex systems, such as non-newtonian fluids and multi-phase flows. For such systems it is especially important to understand the relations between the mean flow characteristics and the local turbulence and mixing properties in order to bring out the effects of anomalous viscosities of suspended phases. It is important, therefore, to investigate the deviations from newtonian behavior using phenomenological view points. In our analysis of the turbulent flow of dilute fiber suspensions we have endeavored to do this also and to integrate the conclusions with the results of statistical examinations.

2. Some Historical Aspects - Isotropy vs. Homogeneity

The statistical analysis of turbulence owes much to G. I. Taylor (1) (2) who did pioneering work in viewing turbulence as a field of fluctuating velocities described by a random continuous function of position and time. His initial work treated the simplest category of turbulent flows, the ideal isotropic turbulence. This is a random motion in which the mean values of the flow variables are independent of translation, rotation and reflection of the axes of references. For isotropic motion the changes in direction and magnitude of fluctuations at a given point are wholly random and there is no correlation between the behavior of the components. Although no turbulent flow in nature is perfectly isotropic, isotropy was taken initially as the model for flow behind uniform grids. Actually such a flow is more nearly homogeneous, i.e., a random motion whose average properties are independent of position in the fluid space, although the statistical properties of the several components of the fluctuations at a point are not completely independent as isotropy requires.

Taylor introduced the concept of correlations between velocities at two points in the fluid to describe the statistical properties of the fluctuations with respect to their spatial distribution and phase relationships. In 1938, Taylor (3) made a further contribution by introducing a result of pure mathematics probably suggested by Wiener (4) in his famous paper of 1930 on generalized harmonic analysis. Taylor's paper uses the fact that for a random function the Fourier Transform of the correlation between two velocities is an energy spectrum function in the sense that it describes the distribution of kinetic energy of the turbulence as a function of the Fourier wave-number components, or (since the wave number is an inverse function of frequency) of the frequency of the fluctuations. The definition of correlation and energy spectra will be discussed in Section II-4 of this report, but we note here that this relation between the two is of double significance. Given one, the other can be computed, or if the two are independently determined for the same time-series, a comparison may disclose otherwise hidden features and possible errors in the time-series.

Following Taylor these methods and extensions of them have been used widely. In the analysis of isotropic and homogeneous turbulence we refer the

reader to Ref. (8) for a general review and to Refs. (5) through (10) for the details of certain aspects. In the case of shear flows, the application of these concepts to instrumentation and analysis is described in Refs. (11) through (15).

3. Turbulent Shear Flows

Turning specifically to turbulent shear flow we note that when there is a variation in mean velocity across a field of turbulent fluid such that a net shear stress exists, there is a variation in the average values of the fluctuating properties. In consequence there are interactions between the mean motion and the turbulent motion, and the phenomenon is more complicated than the simpler homogeneous case. There are gradients of the various properties and there is said to be transport effects as the turbulent energy goes through various stages of transformation. For fully developed steady flow in a pipe there is no decay of mean or fluctuating quantities in the direction of flow, but the turbulence passes through all its stages across the pipe section - turbulent energy production from the mean flow, energy diffusion, and turbulent and laminar dissipation.

In the past various experimental investigations have been carried out in different types of shear flows of single phase fluids. The difference between the so-called free turbulent flows and the flows past solid boundaries has been recognized. It becomes apparent when studying these flows that the dynamic and kinematic processes, which govern, may be completely different. Laufer (11), investigating the flow in a two-dimensional channel, found some results, but these were far from being complete. One consequence of his study was the realization that in order to obtain a complete picture, say of the turbulent energy balance, a knowledge of flow conditions in the close proximity of the wall was of the utmost importance. Later Laufer (12), with an emphasis on turbulent structure, carried out a study in a 10" diameter pipe.

The purpose of Laufer's investigations was to reveal details of flow structure that could not be found from study of mean flow alone. Laufer verified that rates of turbulent-energy production, dissipation, and diffusion have sharp maxima near the edge of the laminar sublayer and that there exists a strong movement of kinetic energy away from this point and an equally strong movement of pressure energy toward it. Also, from the standpoint of turbulent structure, the field within the pipe may be divided into three regions: (1) wall proximity where turbulence production, diffusion, and viscous action are all of equal importance; (2) the central region of the pipe where energy diffusion plays the predominant role; and (3) the region between (1) and (2) where the local rate of change of turbulent-energy production dominates over the energy received by diffusive action.

It is important to realize the additional complexity of turbulent shear flows over the isotropic or homogeneous turbulence. For further information the reader should consult Tchen (13), which is a deep and extensive analytical treatment of the nonisotropic case, and (14), (15). Tchen's work will be mentioned later in relation to spectra shapes.

4. Correlation Functions and Spectrum Density Functions in Turbulent Flow

Two statistical parameters are especially useful in dealing with random processes. They are correlation functions and energy density spectrum functions. As pointed out by Taylor Ref. (3) they are particularly useful in discussing turbulence. In the following subsections we will discuss these functions briefly.

(a) The Stationary Random Process. Consider a phenomenon occurring throughout a field of space. Imagine a series of records taken simultaneously at many points in the space and each extending over some definite time interval. These records of random fluctuations may be averaged in various ways. Suppose that averaging over large numbers of the different records at some time t_1 gives the same result as at t_2, t_3, etc., so that all statistical quantities are invarient with respect to time translations. As defined in Ref. (18) this behavior is known as a stationary random process. In the more general non-stationary random process, this invarience would not be realized. Now, if, in addition, the averages with respect to time at fixed locations turn out to be identical to the averages with respect to location at fixed times, the process is said to be ergodic as well as stationary. Since the records from the turbulence measurements are time functions, if we assume ergodic as well as stationary conditions prevail at any given radius in our circular tube we may use time averages instead of space averages in the analysis of the results. Furthermore, one experimental record should suffice to give the true statistical properties. We will make this assumption in treating the experimental data, but we should remember that it is an assumption which may not hold exactly.

(b) Autocorrelation vs. Crosscorrelation. Two records from a series of different records such as described in the last paragraph may have certain similarities and show some degree of correlation. In a single record the events at different successive times may be more or less related to the happening at the starting time. Such information is obtained by a correlation procedure. Suppose we have two functions of time $x(t)$ and $y(t)$. We perform a correlation if we delay $y(t)$ by an amount τ and then multiply the two functions and average over a time period. If $x(t)$ and $y(t)$ are different we have a time crosscorrelation. If $x(t)=y(t)$, i.e. we use the same record delayed with respect to itself, we have an autocorrelation. For a record $y(t)$ from a random process, the autocorrelation function is defined as

$$R(\tau) = \lim_{T\to\infty} \frac{1}{T} \int_0^T y(t)y(t+\tau)dt \qquad [1]$$

where T = sample length.
For a stationary random process it can be shown that $R(\tau)$ has the following properties:

$R(\tau) = R(-\tau)$ i.e. symmetry about R=(0)

$R(0) = \overline{y^2(t)} > 0$

$R(0) \geq R(\tau)$ but $R(\tau)$ may be $\pm$

Applied to turbulence we will express Eq. [1] in the notation

$$Y_A(\tau) = \lim_{T\to\infty} \frac{1}{T}\int_0^T u'(t)u'(t+\tau)dt \qquad [1a]$$

where u' = x-component of velocity fluctuation.

The results of autocorrelating are customarily represented as correlograms of $R(\tau)$, or (Y_A), plotted versus the delay time τ.

In practice, of course, T cannot be infinite so that experimentally we determine

$$R(\tau,T) = \frac{1}{T}\int_0^T y(t)y(t+\tau)dt \qquad [2]$$

or, applied to turbulence

$$Y_A = Y_A(\tau,T) = \frac{1}{T}\int_0^T u'(t)u'(t+\tau)dt \qquad [2a]$$

Differences can be expected between theoretical and experimental results due to finite sample lengths as well as due to deviations from the truly stationary random conditions.

Applied to turbulence, the autocorrelation at τ=0 gives the rms value of the turbulent fluctuations. If the correlation function is made dimensionless the area of a plot of $R(\tau)$ vs τ gives a relative time scale, an average persistence period for the fluctuation.

The use of time cross correlations in analyzing turbulence would add importantly. This has been done with hot wire instruments in air flows. However, in the present experiments, like in most cases of liquid flow, it is not practical to obtain two simultaneous records. Never-the-less, it would be interesting to cross correlate two records at different radii, even though they were not simultaneously obtained.

(c) The Energy Spectrum and Relation to Autocorrelation. The energy spectrum of turbulence is the frequency distribution of the kinetic energy contained in the fluctuating velocity components of a turbulent field. We

will define the energy* density spectrum function $\Phi(n)$ as the average kinetic energy per unit mass at a point in the flow contained in a given frequency bandwidth Δn divided by the bandwidth. The total average kinetic energy associated with the u'-turbulence at a given point is then

$$\text{Total K.E./mass} = \overline{u'^2} = \int_0^\infty \Phi(n)dn \qquad [3]$$

where n = ordinary frequency, cycles per second

$= \omega/2\pi$

It is convenient in making measurements to use the fraction of the energy in a bandwidth referred to the maximum energy density occurring in the entire spectrum, so we define

$$F(n) = \frac{\Phi(n)}{\propto \overline{u'^2}} \qquad [4]$$

where $\propto \overline{u'^2}$ = the maximum average kinetic energy per unit bandwidth in the spectrum

Inserting Eq. [4] in [3] gives

$$\overline{u'^2} = \int_0^\infty \propto \overline{u'^2} F(n)dn \qquad [5]$$

Then we write

$$\int_0^\infty \propto F(n)dn = \int_0^\infty F_1(n)dn = 1 \qquad [6]$$

where $F_1(n)$ = the fraction of total energy per unit mass per unit bandwidth.

It is customary to present spectra as graphs of $\Phi(n)$, $F(n)$ or $F_1(n)$ versus frequency n. Roughly, the low frequency portion of a spectrum represents kinetic energy of the large eddies of turbulence, and the high frequency portions represent energy in small eddies.

---

* $\Phi(n)$ is often called a power density spectrum since if the random process is represented by voltage fluctuations and a load of one ohm is assumed, $R(\tau)$ has the units of $(\text{voltage})^2$ and $\Phi(n)$ the units of watts per cycle per second.

Spectrum density functions can be determined by different methods. In the present experiments spectra of the outputs from a turbulence gage were determined directly by a frequency analysis using a wave analyzer as described later in this report. Alternately, in the special case of a stationary random process, the energy density spectrum function is related to the autocorrelation function by useful formulae which permit the conversion of one into the other. These formulae are the result of applying classical harmonic or Fourier techniques, and detailed aspects are given in Refs. (3), (4) and (16) through (19). Here we present the main relations and comment briefly.

If $R(\tau)$ is the autocorrelation function of a stationary but not necessarily ergodic random process and the energy density spectrum of the process is $\Phi(n)$, then according to the Wiener-Khinchin relations,

$$R(\tau) = \int_0^\infty \Phi(n) \cos 2\pi n\tau \, dn$$

and [7]

$$\Phi(n) = 4 \int_0^\infty R(\tau) \cos 2\pi n\tau \, d\tau$$

Thus, the autocorrelation function can be determined through a Fourier cosine transform of the energy density spectrum, and vice versa. From Eqs. [1], [6] and [7] we see

$$R(o) = \overline{y^2(t)} = \int_0^\infty \Phi(n) dn = \int_0^\infty \overline{u'^2} F_1(n) dn \qquad [8]$$

or applied to turbulence

$$Y_A(o) = \overline{u'^2} = \int_0^\infty \overline{u'^2} F_1(n) dn \qquad [9]$$

While these relationships hold for the special case of a truly stationary random process we apply the conclusions to interpreting the separately determined autocorrelation and spectrum density functions for the experimental records from the turbulence tests.

5. Some Practical Considerations of the Autocorrelation Function

There are several kinds of statistical errors that may be encountered

in the measurement and analysis of random time functions. From the extensive literature discussing these we have included items (16) through (23) in the list of references. In the following we comment specifically on some effects having bearing on our measurements.

(a) Periodic Phenomena. If an otherwise random signal contains a periodic component, this periodic component will persist at large delay times, while the random components tend to average out. Following Ref. (18), pg. 24, this may be shown as follows.

Let a single record of a stationary (not necessarily ergodic) process be

$$y(t) = A \sin (2\pi nt + \phi) \qquad [10]$$

where A = constant

ϕ = phase angle = constant

n = ordinary frequency, cycles per second = $\frac{\omega}{2\pi}$

ω = angular frequency, radius per second

In Eq. [1] replace $R(\tau)$ by $R(\tau,y)$ to indicate dependence on $y(t)$ so that

$$R(\tau,y) = \lim_{T\to\infty} \frac{A^2}{T} \int_0^T \sin [2\pi nt + \phi] \sin [2\pi n(t+\tau) + \phi]dt$$

$$= \frac{A^2}{2} \cos 2\pi n\tau \qquad [11]$$

We see $R(\tau,y)$ is

a) independent of phase angle ϕ

b) is an even function of τ

c) has a maximum at $\tau=o$

d) is periodic in τ with the frequency of the original record $y(t)$.

If then a record contains periodicities superposed on a random signal, they should be detected by calculation of $R(\tau,y)$ for large delay times. Otherwise for large τ, $R(\tau,y)$ would be expected to go to zero.

(b) Effect of Sample Length. If as in practice the sample length T is finite, there arises the question of the accuracy of the process of autocorrelating. This question has been treated in several references. For example, see Refs. (18) to (23) inclusive. The problem is to determine under what circumstances the experimentally determined function

$$R(\tau,T) = \frac{1}{T}\int_0^T y(t)y(t+\tau)dt \qquad [2]$$

converges to $R(\tau)$ as defined by Eq. [1]. The important difference between Eqs. [2] and [1] is that T is finite in [2], making the correlation R a function of both τ and T.

It has been proven theoretically that as T approaches infinity, $R(\tau,T)$ does converge, in the mean, to $R(\tau)$. The manner in which it converges is, however, unknown as yet. It is conceivable that $R(\tau,T)$ converges to $R(\tau)$ in some oscillatory manner and there exists an optimum length T or set of optimum lengths. Tukey (24), (25) pointed out some errors of finiteness of record length which are strongly dependent on the distribution of the particular random variable involved. Weiss (23) has shown that a narrow band of Gausian distributed noise leads to the prediction of a long-term cyclic behavior in the correlogram.

(c) Waxing and Waning. It has been observed and reported [e.g. Refs. (23), (27)] that at large delay times some autocorrelograms show a disorderly increase and decrease of the envelope. This is known as waxing and waning. A possible cause is a periodic signal plus some corrupting signal. Another possibility places this as an error of the finite sample correlation process. This possibility was demonstrated by Weiss (23) as will be described in later discussion of our experimental results.

III. DATA MEASURING AND PROCESSING: EQUIPMENT AND PROCEDURES.

1. Test Loop and General Procedures.

The turbulence measurements and velocity profiles were taken at the downstream end of the 2-inch diameter horizontal loop described in Ref. (29). The probe tip was flat faced. Some of the earlier runs reported in Ref. (29) used a 0.15-inch diameter tip. All subsequent tests used a 0.25-inch diameter tip. The probe projected into the end of the 2-inch conduit a distance of 2.75-inches from a streamlined cross-flow support. The support spanned the full 2-inch diameter so that the resistance caused by the probe did not change with probe position. Initially, an extending lower lip was attached to the conduit behind the probe support to maintain hydrostatic pressure distribution as long as possible so that the probe tip would not be in the zone of transition from hydrostatic to the uniform (zero) pressure existing in the emerging free jet. Later with high concentrations at the highest flow rates, the free-jet discharge resulted in severe air entrainment. A flexible extension was added to the end of the 2-inch lucite tube which connected into the three-way diversion plug valve used for flow deflection from the stock reservoir to the calibrating tank. This allowed a submerged discharge into the reservoir [See Section 4.3 of Ref. (29)]. It also made volumetric flow determinations more easily possible. The extension was used particularly in making velocity traverses. However, for turbulence traverses it being necessary to isolate the turbulence probe and gage from the general vibrations of the test loop pipe, the free jet discharge was more suitable and was used. To extend the turbulence measurements to higher concentrations and velocities this problem of instrument isolation versus air entrainment and foaming will require more attention in the future.

The suspensions were circulated by a variable speed Gould open-impeller centrifugal pump. An open steel tank equipped with a propeller mixer served as stock supply reservoir and pump head tank. One end of the tank comprised the volumetric discharge measuring compartment. In operation the flow rate was computed from a pressure drop measurement along the length of the pipe using a conversion established by calibration tests giving flow rate versus pressure drop for each pulp and concentration conbination.

2. Turbulence Gage and Data Recording

The gage used for the turbulence measuring investigation was developed at the M.I.T. Hydrodynamics Laboratory for the study of turbulence in high-velocity free-surface flow. This gage, described in detail in Ref. (36), consists of an impact probe connected to a capacitance pressure transducer.

The impact tube senses fluctuations in the stagnation pressure. Eliminating the mean hydrostatic head at the probe tip there remains

$$H = \frac{(\bar{u}+u')^2}{2g} + \frac{p'}{\gamma} = \frac{\bar{u}^2}{2g} + \frac{\bar{u}u'}{g} + \frac{u'^2}{2g} + \frac{p'}{\gamma} \qquad [12]$$

where H = instantaneous dynamic head

$\bar{u}$ = local mean velocity

u' = x-component of turbulent velocity fluctuation

p' = local turbulent pressure fluctuation

In this relation p'/γ and $u'^2/2g$ are terms of the same order of magnitude but normally out of phase. The term $\bar{u}^2/2g$ is a constant. Thus the fluctuating component of H, and the output of the capacitance transducer, is dependent primarily on $\bar{u}u'/g$. This relationship is assumed to hold exactly in the use of the instrument. A discussion of the possible magnitudes of errors is given in Ref. (36).

Fluctuations of the stagnation pressure at the tip of the probe are transmitted to a relatively stiff 0.042-inch thick diaphragm in the transducer. This diaphragm is, in turn, separated from a brass cap by an air gap. The air gap has a thickness of 0.001-inches. The diaphragm forms one plate of a two-plate capacitor, connected to a parallel-resonance tank circuit. The circuit is tuned when the diaphragm is in its neutral or zero pressure position, that is, when the air gap is 0.001-inches. Defections of the diaphragm under the action of pressure fluctuations detune the tank circuit, causing voltage fluctuations in its output circuit. The voltage fluctuations are then amplified to a suitable level for measurements. The amplified variations can be made visible either on an oscilloscope or the variation can be stored on a magnetic tape for subsequent processing. Some changes were made in the circuiting from that described in Ref. (36). Most importantly, the original amplifiers were replaced by a more stable unit, and this in turn mounted directly on the capacitance pressure cell unit to eliminate connecting cables and associated signal transmission problems.

Turbulence gage data was recorded for later processing. In this step the amplified output of the tranducer was further amplified by a factor of 10 using a Glennite Model F-408 A.C. coupled Decade Amplifier. The final signal, containing essentially only the fluctuating voltage components, was placed on magnetic tape.

The recordings were made using two tape machines. The first, an Ampex Model S-3175 is a seven-channel FM carrier type, employing a 1-inch tape, and designed to record and reproduce data from DC to 5,000 cycles. It is a three-speed unit operating at 0.3, 3.0, and 30.0 inches per second tape speed on record and intended to play back only at the 30-inch speed. In the recording process, the input signals frequency modulate a pulse generator, the pulses being recorded on the magnetic tape. The pulse generator can be switched for any of three carrier frequencies; 270, 2700, or 27,000 cycles $\pm$ 1% for operation with 0.3, 3.0, and 30.0 inches per second tape speeds, respectively. Only two playback amplifiers are provided. Either or both can be connected to any of the seven playback beads through a special switching panel. The frequency response when recording at 0.3, 3.0, 30.0 inches per second and playing back at 30 inches per second tape speed, is:

± 1/2 db 0 to 3,000 cycles

± 1 db 0 to 5,000 cycles

The second recorder used was an Ampex Model 306-2 two-channel FM carrier type employing a 0.25-inch tape. Both machines were used with the 30.0 inches per second recording speed, and at that speed had the same characteristics.

During an experiment the amplified output of the capacitance gage was sent to both the left channel of an oscilloscope and to the input of the Ampex recorder. The output from the Ampex was then fed back into the right channel of the oscilloscope. This procedure, of looking at both the input to the Ampex and the output from the Ampex, is desirable in order to insure reliability of the recording. The recording speed as well as the reduction speed on the analog correlation were both 30 inches per record, therefore making the speed-up ratio 1 to 1.

The utmost precaution had to be observed in mounting the gauge because of its very high sensitivity to external vibration. The test stand on which the gauge sets is separated by sponge rubber from the concrete floor. The table on which the oscilloscope, the one amplifier, and the solar sets, was placed upon sponge rubber mounts. A sheet of sponge rubber separated each piece of equipment from the table. Even though many precautions were taken to reduce the noise-to-signal ratio, a small fraction was present. This fraction was considered negligible.

Special precautions had to be observed in filling the gage including the impact tube to make sure no air was trapped in any part of the internal mechanism. Unless all the passages and cavities are water filled the gage response is affected by a falling off of the effective resonant frequency of the unit. In early experiments each gage component was flushed with a detergent using a hypodermic syringe and needle. The components were then assembled under water which had been deaerated by boiling or by vacuum. The filling techniques were improved during the course of the experiments. In the procedure finally adopted, a large vacuum tank was employed within which the disassembled components of the entire gage unit could be immersed in water. After applying a high vacuum for a period of six to eight hours the gage was assembled under water.

The natural frequency of the gage unit, including the impact tube, was reported to be about 90 cps in Ref. (29). This is thought to be low, probably due to the presence of some undissolved air. Subsequent determinations of the resonant frequency, with a longer impact tube, but after the gage had been filled by the improved procedures, gave values in the range of 160 to 190 cps. The computed effect of the different tube diameters and lengths is to change the resonant frequency by about 10 %. Thus with the unit properly filled with water the resonant frequency should be of the order of 150 cps or greater. With poor filling it is probably less.

3. The Correlator and Autocorrelation Procedures.

The processing of data into autocorrelation curves was carried out by the Analog Correlator (28) of the Communications Biophysics Laboratory and previously described in Ref. (29). This equipment was made available without cost to this TAPPI project. The correlator calculates the value of the integral

$$\frac{1}{T}\int_0^T y_1(t)y_2(t+\tau)dt \qquad [13]$$

for discrete intervals of τ. With $y_1 = y_2$ an autocorrelation is performed according to Eq. [2].

The two signals to be correlated are recorded on adjacent tracks of a magnetic drum. The delay is achieved by sending the two signals from read heads that are displaced along the circumference by a distance proportional to the value of delay. The multiplier is a quarter-square device and the integrator is a simple Miller integrator. Thus, to get an autocorrelation curve by this method, it is necessary to record the data on a magnetic tape. Reflectors are then taped onto the magnetic tape, separated by a distance along the tape proportional to the sample length (T). The correlator can then be set to make automatically one pass over the data (from reflector to reflector) for each point on the autocorrelation curve. The beginning and end of the sample are sensed by shining a light on the tape. When the reflection is reached, a photo-electric cell produces a pulse, triggering control relays that rewind the tape, start the correlator, and stop the correlator.

The overall characteristics of the system are dependent on the components used in the recording of data, and on the ratio of playback speed (during analysis) to the recording speed of the magnetic tape. The characteristics for the case in which there is no speed-up of the tape during analysis, that is, when playback for analysis is at the same speed as that of the original recording, are as follows: maximum overall bandwidth, 1 cps to 5 kc/sec; maximum delay, 185 m sec; number of possible $\Delta\tau$ (the units by which τ is changed for computation of successive points of the correlation function), 30, ranging from 1/16 m sec to 10 m sec, maximum length of record which can be analyzed (T), 50 seconds.

Control runs have been made in the analog correlator in order to insure that no errors result from the machine processing of the data. A typical control run is the autocorrelation of a 250 cycles per second sinusoid. There is no significant change in the period of the sinusoid as a function of delay. Thus, it is reasonable to conclude, that the machine errors can be assumed to be second-order effects.

4. Energy Spectra Measurements.

To obtain a spectrum analysis of the taped records of the turbulence gage output a General Radio Type 762-B Vibration Analyzer was used. This is a narrow-band, constant percentage bandwidth, analyzer and is continuously

tunable from 2.5 to 750 cps. The output for any bandwidth is the average intensity of the incoming signal over the frequencies within the bandwidth as a fraction of the maximum average intensity occurring for any bandwidth in the entire spectrum. The output as read on a vacuum tube voltmeter (an integral part of the analyzer) is then

$$F_1(\Delta n) \backsimeq \frac{\sqrt{\overline{u'^2}_{\Delta n}}}{\left[\sqrt{\overline{u'^2}_{\Delta n}}\right]_{max}} \qquad [14]$$

where Δn denotes a given bandwidth. To convert to the spectrum level that would be measured if the analyzer had an ideal response characteristic with a bandwidth of 1 cycle, a correction (specified by the instrument manufacturer) is applied to each voltmeter reading. Applying the correction, which is a function of frequency (and hence bandwidth) and denoted by $C(\Delta n)$, and squaring gives

$$F(n) \backsimeq [F_1(\Delta n) - C(\Delta n)]^2$$

$$\backsimeq \frac{\overline{u'^2}_n}{\overline{u'^2}_{max}} \qquad [15]$$

The spectrum data is presented as plots of $F(n)$ versus frequency n.

The method used in obtaining a signal to feed into the wave analyzer will now be described. As stated before, the output from the capacitance gage was permanently recorded in the Ampex tape recorder. For convenience the tape was then placed in the analog correlator and the correlator was set in motion and allowed to wind and rewind, i.e., complete its natural cycling. The wave analyzer was set to a certain frequency and as the tape then went through its winding cycle, the instrument meter reading was taken. The estimated accuracy of this reading is ± ten percent. The tape then rewound, the wave analyzer was set at another frequency, and the process repeated for another wave analyzer reading. This process was continued until the entire frequency range was exploited. The process gives averages of the intensity of the fluctuations requiring a subsequent squaring to obtain energy units. Alternately the output of the autocorrelator at zero time delay (τ=o) would give an energy function directly to feed to the analyzer. This was not conveniently possible at the time of the experiments, requiring special connections to the correlator which had been made available in between other scheduled uses.

5. Turbulence Gage Calibration.

When the correlating procedure is carried out by the analog correlator,

the ordinate (τ=o), gives the value of the mean square ($\overline{u'^2}$) of the turbulent fluctuations. A calibration is necessary, if one wants to determine absolute values of the fluctuations. In Ref. (29) magnitudes were approximated by relating the slopes of the corresponding velocity profiles to the autocorrelation results and assuming the same relationship between rms of the u'- and v'- fluctuations and $\overline{u'v'}$ as found by Laufer [Ref. (12)] for air. Subsequently, efforts were made to experimentally determine an overall calibration factor. This matter was one of the most difficult to accomplish with reliability and was not really solved to complete satisfaction. A procedure was evolved which, in principle, should give useful calibration factors, but which requires considerable developmental investigation to assure it practical usefulness. The method involved the application of a known sinusoidal pressure pulse to the tip of the pressure probe, recording the pulse on tape and then autocorrelating. The ratio of the mean square value of the applied pulse to the square root of the correlogram ordinate at τ=o is the calibration factor.

A block diagram of an electro-mechanical arrangement to effect a calibration is shown in Fig. 1. A mechanically-linked system drives a piston in a sinusoidal motion. The piston is soldered to a diaphragm, the diaphragm acting as one end of a closed pressure chamber. The mechanical arrangement is such that both the amplitude and the frequency of the piston can be varied. The capacitance gage probe is inserted through the other end of the pressure chamber, and a seal is placed around the probe to insure a rigidly contained chamber. The remaining electronics of the calibration setup are identical with the arrangement used in recording velocity fluctuations.

With this arrangement the response at the probe is nearly, but not exactly, sinusoidal. Reflections within the pressure chamber modify the applied sine wave pressure pulse.

In operation, the signal from the capacitance gage and the output from the Ampex recorder are simultaneously observed on a cathode ray oscilloscope. As in the case of data recording, the procedure of looking at the signal before and after the recording is advisable in order to insure a valid operation of the Ampex recorder. The peak to peak voltage of the near sinusoid, on the oscilloscope, is recorded. The gage is then calibrated statically. A static pressure head is applied, until it reaches such a height, that it causes a similar voltage deflection as the peak to peak recorded voltage of the applied pressure sinusoid. The peak to peak value, of a sinusoid, is easily connected to a root mean square, and then a mean square value.

The final step is to autocorrelate the tape record from the calibration run, for which we can now evaluate the ordinate at τ=o as the mean square of the pressure pulse. Assuming the random signal of turbulence and the near sinusoidal signal produce the same response in our measuring system, we have a calibration and can evaluate all the other ordinates of the autocorrelogram.

In this procedure the frequency of the applied pressure pulse n as well as the delay time interval $\Delta\tau$ and sample length T used in autocorrelating are variables that may affect the calibration factor obtained. Following the

development of the procedure it was possible to complete an overall calibration for only one set of these three variables; namely n=12.2 cps, $\Delta\tau$=2 milliseconds and T=18 seconds. The result gave a calibration factor of 2.35 which when multiplied by the ordinates Y_A at τ=o gives magnitudes in inches per second. This factor was used to obtain the magnitudes shown in the plots of Figs. 10 and 11. As will be described further on discussion of the results, there are some anomalies in the apparent rms values which suggest that the calibration factor may not be constant. This matter requires further investigation and development.

6. Mean-Velocity Measurements.

The mean-velocity* measurements in the suspensions investigated in the present report were made using essentially the same equipment and same procedure described in the previous report (29),[Section 4.4].

The impact tube had a blunt, circular face,0.25" in diameter and with a 1/16" opening, tapering off to a cylindrical stem of 1/8-inch diameter. The blunt shape had been found effective in preventing fibers from gathering at the tip. The size of the required tip diameter appeared to be a direct, but unspecified, function of fiber length and concentration. Provisions were made for flushing the tube, as well as the static pressure openings, which were located at the two ends of the horizontal diameter and at the upper end of the vertical diameter of a section approximately one inch upstream of the tip. The dynamic and static pressure openings were connected to an inverted-U air-water manometer.

In general, during the present experiments it was found that Groundwood fibers had a less pronounced tendency to collect at the tip of the impact tube than the Long Lac 17 fibers. However, considerable difficulties were experienced with the Groundwood suspensions on account of finer particles penetrating occasionally inside the tube. The particles could be flushed out at times only with great difficulty, owing to an expansion of the internal passages of the impact tube immediately after the tip opening. No similar difficulties were encountered with the Long Lac 17 suspensions.

The velocity traverses were taken starting at the centerline, and moving toward the wall (in order to operate at progressively decreasing impact pressure, and hence with water flowing out of the tube, thus reducing the possibility of internal clogging). From the wall, the probe would be returned directly to the centerline, when a new check reading would be taken, and then moved toward the opposite wall, to check the symmetry of the velocity profile along the whole diameter.

---

* By mean-velocity we denote the time-average of the fluid velocity at a given point in the fluid; by average velocity we denote the average bulk velocity, i.e., the overall discharge through the cross-section, divided by the area of the cross-section.

IV. EXPERIMENTAL RESULTS AND ANALYSIS

1. Experimental Variables and Scope of Tests.

In the previous phase of this research, which was reported in Ref. (29), an exploratory study of the turbulence characteristics and velocity distribution of fiber suspensions was made. The study was confined to suspensions of one natural fiber only, Long Lac 17, tested at one flow rate ($R \simeq 1.60 \times 10^5$). The results were related to the results of pressure drop measurements (which were performed over a wide range of flow rates and concentrations with suspensions of three natural fibers, Long Lac 17, Coosa River 55 and Poplar Groundwood). In the present experiments the turbulence and velocity measurements covered a range of flow rates and were extended to suspensions of another natural fiber, Poplar Groundwood.

The two fibers investigated in the present report represent the two extremes in the characteristics of the three natural fibers for which pressure drop measurements are available from the previous report. The Long Lac 17 fibers are the longest and most flexible, and their suspensions showed the greatest deviation from the friction factors for water at the same flow rate. The Groundwood fibers are the shortest, and least flexible, and their suspensions exhibited the smallest deviation from the water friction factors. The principal characteristics of hydrodynamics importance are given in Table I for these two fibers. The results of pressure drop measurements are given in Figs. 2 and 3 (which are Figs. 15 and 19 from Ref. (29)).

The present measurements were aimed at covering the two extreme flow rates in the turbulent range; namely, a flow rate slightly higher than that at which the transition regime ends, and the highest flow rate for which head loss measurements were available. Also, in some cases, measurements at an intermediate flow rate were deemed necessary. For Long Lac 17 some of these measurements were already available from the previous report, having been performed at a flow rate which corresponded to an intermediate point of the turbulent range.

It was not always possible, on account of clogging or other experimental difficulties, to perform measurements at all the desired flow rates (particularly the turbulence measurements); at other times, some of the intended measurements appeared superfluous, because a clear enough picture of the flow phenomenon had already emerged from previous measurements.

The Reynolds numbers and concentrations for which turbulence and mean-velocity data were taken, are given in Table II. In conformity with previously reported data, the Reynolds number in Table II and throughout this report are based on the water viscosity for the temperature of the suspension. A comparison of the values in Table II with Figs. 2 and 3 shows the locations of the test conditions relative to the transition and turbulent flow regimes.

2. Turbulence Measurements.

The turbulence data recorded on the magnetic tape were all analyzed in terms of their autocorrelation function. In addition, for water and for 0.5 % solutions of both Long Lac 17 and Poplar Groundwood, energy density spectra were obtained, each at a Reynolds number well into the turbulent flow regime. Typical autocorrelograms are shown in Figs. 4 to 6 as Y_A versus delay time τ in milliseconds (Eq. [2a]). The energy spectra for water and the two solutions are plotted in Figs. 7 to 9 as F(n) versus frequency n in cps (Eq. [15]).

In the following subsections, after presenting some of the specifics of the data taking and analysis procedures we will discuss in a general way the results of the autocorrelations and spectral analyses as to their interpretation and in relation to their disclosing information about turbulence. In Section IV-3 we will consider the findings and conclusions as regards the turbulent processes particularly.

(a) The Test Data. In recording the turbulence data on the magnetic tape, about 5 seconds at 30 inches per second tape speed were allowed to obtain steady tape motion. Following this, records ranging in length from 30 to 60 seconds were obtained (for a particular suspension, velocity and probe position). Care was taken by monitoring each recording to assure the gage output was "uniformly random" so far as could be determined visually, so that no obvious periods of probe blockage with pulp would be included. In some cases, notably on the pipe centerline with Long Lac 17 at 0.75 % and 1.0 %, records as long as 30 seconds could not be obtained without intermittant steady stretches. This is not believed due to ordinary fiber clustering on the probe tip, but is interpreted as evidence of intermittant plug-like flocs persisting at the pipe axis. Were this due to fiber clustering the same kind of record should have been obtained at the other radii which was not the case.

In autocorrelating, all the data was initially processed using step increments in time delay of 2 to 2.5 milliseconds. For Groundwood, however, the presence of a periodicity of especially high frequency (to be discussed) necessitated much smaller steps, and all the Groundwood recordings were reprocessed using 0.25 millisecond increments.

The initial autocorrelograms for water and Long Lac 17 were obtained using a sample length T of 10 seconds selected from the longer total record. Later many of the correlations were repeated using T=20 seconds. The starting points of the 10-second samples were not identified so the 10- and 20- second samples did not start at the same point. Sometimes the 20-second sample overlapped the 10-second one, but never completely. The Groundwood data was all processed using T=20 seconds and a few selected runs were processed using 10, 20, 30 seconds or 20, 30, 45 seconds.

The length of sample used for a frequency analysis was approximately 30 seconds. This 30-second sample overlapped (to varying extents with the water and two solutions) the samples used for autocorrelating.

The information about intensities derived from the autocorrelograms is summarized in Table III, which gives the ordinates Y_A at the origin (i.e., at τ=o). The various sample lengths T used in correlating are shown for each of the several suspensions and Reynolds numbers of the tests. It will be recalled that the ordinates of the diagrams (unnormalized) at τ=o are proportional to the mean square of the fluctuations. The tabulated values will give the true mean square values when multiplied by a calibration factor as described in Section III-4.

(b) Features of the Autocorrelograms and Energy Spectra. First, there are several features appearing in the records which have general significance. They are as follows:

1. Each autocorrelogram shows some regular periodicities persisting through large delay times.

2. In some cases, as shown by the example in Fig. 6, the envelope of the maximum ordinates in a correlogram shows some oscillations, or "wax and waning" as previously defined, at large delay times.

3. The magnitude of the correlation factor at τ=o depends on sample length T. The magnitude generally is higher for longer sample length.

4. In each case the energy spectrum shows a non-uniform energy distribution with distinct peaks at two or more frequencies.

5. The Poplar Groundwood gives odd results, (a) the τ=o ordinate of the correlograms exceed those for water and Long Lac 17 by a large amount. (b) Each energy spectrum shows a large hump centered at 150 cps which does not appear with water and Long Lac 17.

Turning to more specific points, it was found that the regular fluctuations present in the autocorrelation records have, for a given run and probe position, a practically constant period or time interval T_p between two successive peaks. The frequency equivalent of these periods, designated by ω_o, are listed in Table IV for all the runs for which a sufficiently long correlogram was available. Also shown are the frequencies corresponding to the major peaks in the energy spectra. With aid of this table we summarize the following points about the periodicities:

6. There is practically no variation in ω_o with radical position of the probe.

7. There is no definite variation in ω_o with sample length T.

8. Only for water is there a variation in ω_o between tests at different

Reynolds numbers, but it is irregular and indefinite.

9. There are conflicting trends in ω_o with concentration, slightly downward with Long Lac 17 and slightly upward with Groundwood.

10. For Groundwood ω_o ranges from approximately 143 to 190 which is several times that observed for Long Lac 17 or for water.

11. In each of the spectra for water and for Groundwood one of the energy peaks has a frequency matching ω_o in the corresponding correlogram.

(c) Groundwood Anomalies. Before proceeding with a general discussion let us first consider the anomalous results for the Poplar Groundwood as given in Item 5 of the preceeding summary. Using the same calibration factor for all the suspensions, the higher Y_A at τ=o indicates much higher turbulence intensity, and hence more efficient momentum exchange and higher ϵ values, for Groundwood. As will be seen later, this is contradicted by the experimental velocity profiles which yield ϵ values close to those for water. Thus we infer that either a different calibration factor should be used for Groundwood, or that there is a special factor introducing an error of extra apparent energy into the record. Here we note that since the integral of the energy density spectrum is proportional to the correlation function at τ=o (by Eq. [8]), the extra hump in the Groundwood spectra at 150 cps is the main cause of the higher apparent turbulence. Moreover, this hump is at the frequency of the regular oscillation ($\omega_o \simeq$ 150 cps) observed in the correlogram for the same concentration and Reynolds number. It is believed the hump and the corresponding regular periodicity are due to an excitation of the natural frequency of the pressure cell which did not occur with water or with Long Lac 17. By Item 10 of the above summary, the ω_o values for Groundwood are several times higher than for water or Long Lac 17. It is this high frequency periodicity that required rerunning the autocorrelations as previously described. We note also that at 0.75 % and 1.00 % the Groundwood gives ω_o values of approximately 160 and 190 cps respectively. We have no spectra and hence no check on these frequencies, but since they fall in the range of the gage's resonant frequency as discussed in III-1 it is believed they also are associated with resonant phenomena.

It is concluded that the Groundwood records give incorrect mean square values. However, even at natural frequency operation the magnitude of the diaphragm oscillation is proportional to the force causing it. Assuming the characteristics of the exciting force are the same from test to test, the relative trend of the Y_A values for Groundwood should give an indication of the relative turbulence intensities at different radii velocities and concentrations. With this assumption the data will be examined for its relative indications in Section IV-3.

(d) Periodicities and Waxing-and-Waning. Considering the general question of the regular periodicities in the correlograms, they may be due to (a) resonance in the pressure cell as suspected for the Groundwood, (b) non-turbulence impulses transmitted to the pressure cell such as might be imposed by the pump's rotation or by vibration of the pressure probe itself, (c) some feature of the turbulent flow such as regular oscillations in the wake of the probe, or at zones of flow separation in the conduit system, (d) an inherent feature of the statistical averaging treatment used for data which is complex but not necessarily uniformly random in frequency and magnitude, (e) an inherent property of the local turbulence itself.

As shown in Table IV all the observed values of ω_o for water and Long Lac 17 were well below any reasonably expected resonance frequency of the gage and probe unit. This is not believed to be the cause of the periodicities in these cases.

Considering next the pump as a possible source of regular impulses, we have listed in Table IV the frequencies of rotation Ω and corresponding frequencies Ω_b of pump rotor vanes passing the volute tongue (cutwater). Pump rpm data were not taken during the turbulence tests, but were taken during some of the water and Groundwood velocity profile test runs. The values in Table IV were taken from the latter where available for matching test Reynolds numbers. There appears to be no definite correlation between these pump excited frequencies and the correlogram periodicities. The one comparison for water shows pump imposed frequencies of 11.2 and 56 cycles per second, versus the value $\omega_o \lesssim 30$ from the correlogram. For the 0.5 % Groundwood, the pump frequencies are 11.6 and 58 or 20.8 and 104, versus $\omega_o \lesssim 150$ from the correlogram. For the 0.75 % Groundwood, the pump gives 20.8 and 104, while the correlogram gives $\lesssim 160$ cps. There does not seem to be a consistant combination among the several possible comparisons.

Mechanical vibrations of the probe itself would probably be the result of coupling with periodic pressure oscillations in the wake of the probe. However, it would be expected that the period resulting from either of these two possibilities, whether related or independent, would change with location of the probe in the pipe due to variation in local velocity and hydrodynamic loading. Since ω_o does not vary with probe position nor consistently with Reynolds number (Items 6 and 8 in IV-2b), probe vibrations and wake pressure oscillations seem unlikely causes of the observed periodicities. Admittedly, however, further information is necessary to completely rule out these as causes.

There remains the possibility of some other zone of separation with a periodic wake behavior. However, here too changes in Reynolds number should result in a more definite change in frequency than observed.

With regard to the statistics used in analyzing the data, the fact that a correlogram, in virtue of its finite sample length, is only an approximation to the correlation function, has already been mentioned in Section II-5b.

Recently, Weiss (23) analyzed the autocorrelograms of brain waves, which, as the autocorrelograms in the present experiments, exhibit periodic fluctuations, and an apparently random "waxing and waning" of their envelopes at large delay times. Weiss has suggested that the periodicities and "waxing and waning" are a consequence of the finite sample length, rather than a property of the brain wave. In support of his thesis, Weiss shows that the autocorrelogram of a narrow-band Gaussian noise (a noise generated using a noise source and a quadratic wave filter, and characterized by a theoretical correlation function which should decay rapidly, without waxing and waning), shows the same pattern of the brain waves' correlogram. Weiss' argument does not offer conclusive proof, however, that the periodic phenomena in the brain-wave correlogram - and, analogously, in our records - are a consequence of the finite record length. In our experiments the changes in sample length produced no definite and consistent changes in ω_o. (Item 7 in IV-2b). Neither were we able to correlate waxing-and-waning with sample length. Thus we cannot rule out the possibility that periodic phenomena in our correlograms are a property of the turbulent process itself.

While we cannot advance any hypothesis on the physical nature - and meaning in terms of the turbulent process - of a periodic component of the turbulent field, we must point out that even a weak component would result in periodic fluctuations of the correlogram, consistent with what we observe in our records. However, the observed near-constancy of the period at different radii and for different Reynolds numbers (or, for water, the random variation with Reynolds number) weakens the hypothesis that the fluctuations are inherent in the flow.

We conclude this examination of the factors which may have caused the periodicities, by saying that on the basis of the information available, we cannot single out with certainty specific causes. For the Groundwood suspensions there is a strong indication that gage operation at its natural frequency is one of the contributing factors.

(e) Effect of Sample Length. In the previous subsection, the finite sample length was considered one of the possible causes for the periodic anomalies of the autocorrelation records. While it was not possible to point out with certainty to the finite length as the reason for the anomalies in periodicities, Table III shows that the sample length affects, unquestionably, the ordinates of the autocorrelograms at τ=o, longer sample lengths corresponding to larger ordinates. It was pointed out already that as the sample length T increases the autocorrelogram becomes a better approximation of the theoretical correlation curve. It was also pointed out, however, that the convergence process as T increases could be characterized by oscillations of smaller and smaller amplitude around the theoretical curve. The characteristics and speed of the convergence process depend on the characteristics of each set of data. We can note from a comparison with Laufer Ref. (2) (to be presented later in Figs. 10 and 11) that the data for water when reduced to apparent rms values using the calibration factor described in III-4 gave lower values than Laufer reported for his air studies. With sample length

increase from 10 to 20 seconds the agreement improves. As a consequence it was concluded that the 20 second sample length with the calibration factor which was obtained using T=18 seconds represented the most reliable magnitudes. In the subsequent comparisons of data, the 20 second sample length correlations have been used wherever available.

As previously mentioned the sample length T for the spectra was about 30 seconds. Longer sample lengths would be better since a more accurate mean value of the intensities in each bandwidth would be obtained. This would be most apparent in the low frequencies, say below 5 cps. It is believed this may be a factor in the erratic behavior observed in the spectra plots at the lowest frequencies. Otherwise it is not believed that increased sample length will materially change the spectra obtained with the analyzer and procedures used.

3. Turbulence in Suspensions - Comparison with Water.

(a) Turbulence Intensities. The turbulence intensities as derived from the τ=o ordinate of the autocorrelograms are plotted in Figs. 10-12 versus relative distance from the pipe wall. In Figs. 10 and 11 for water and Long Lac 17 the results of correlating with both 10- and 20-second sample lengths are included. In Fig. 12 where the fiber suspension and water data are compared, 20-second sample lengths were used when available; otherwise a 10-second sample length value was used. In all these figures the Laufer [Ref. (12)] data obtained with hot wire anemometers for air in a 10-inch pipe are included for comparison purposes.

For water and Long Lac 17 the measured quantities have been converted into the dimensionless magnitudes $\sqrt{\overline{u'^2}} \Big/ \sqrt{\tau_w/\rho}$ which are used for the ordinates in Figs. 10 and 11. The procedure for converting to $\sqrt{\overline{u'^2}}$ is that given in Section III-4. The Poplar Groundwood magnitudes, on account of being anomalously high, are represented only as ratios relative to centerline values. This ratio, written as $\sqrt{Y_A} \Big/ \sqrt{Y_{A_\ell}}$, is the ordinate in Fig. 12. In both of these representations we assume that the τ=o ordinate of the correlograms, are proportional to the rms of the turbulent fluctuations and the true value depends only on a calibration factor. With this assumption the values in Fig. 12 are independent of calibration and directly comparable.

First we note some general trends for which the data shows only one or two exceptions:

1. The apparent rms intensities for the water and the suspensions are generally lower than reported by Laufer.

2. The apparent rms values tend to increase from the pipe centerline towards the wall but at a lower rate than shown by Laufer.

3. The main exception is the case of 0.5 % Long Lac 17 at Reynolds number = 1.86 x 10^5. This data gives values higher than the water results and roughly the same as Laufers.

Here the Laufer data is taken as a standard of comparison as it represents the most thorough turbulence investigation of a newtonian fluid using well established hot-wire anemometer techniques. Our generally lower apparent rms values for water may be due to some experimental error, some error in evaluating the data such as a sample length effect or an improper calibration factor, or may represent some real hydrodynamic difference. The difference in radial distribution may be affected, in our case, by the relatively large size of the probe tip (0.25-inches in a 2-inch duct).

Among possible experimental errors, we should consider the effect of any incorrect evaluation of the frictional velocity. As mentioned in Section III-1, in the turbulence rms the rate of flow was computed from a pressure drop obtained by applying a connection coefficient to the measured pressure drop. Values of the ratio $\sqrt{\overline{u'^2}} \Big/ \sqrt{\tau_w/\rho}$ in Figs. 10 and 11 which are too low would correspond to too high frictional velocities, and hence to too high pressure drops (i.e., to an overcorrection of the measured pressure drops). The difference between measured and expected pressure drops in the horizontal pipe being of about 10 %, the uncorrected ordinates of the ratios $\sqrt{\overline{u'^2}} \Big/ \sqrt{\tau_w/\rho}$ would be approximately 6 % higher than shown in Figs. 10 and 11 ($\sqrt{\tau_w}$ being proportional to $\sqrt{\Delta H}$). Assuming 6 % to be the maximum possible spread on either side of the lines in Fig. 10 an ultra cautious assumption - it is obvious that an incorrect evaluation of the frictional velocity could not possibly account for the low values of the turbulent intensities in comparison to Laufer's results.

Thus the low values must either be attributed to an error in the operation of the gage or in the analysis of the data, or must be considered a characteristic of the flow. If we were to extrapolate the trend toward higher rms values as the sample length increases, the data would move closer to Laufer's results. However, we have already discussed in the previous section how we do not know in what fashion, as time increases, the correlogram approaches the theoretical correlation function, so that we cannot legitimately extrapolate the present results. On the other hand, it is interesting that there have been other reports of differences such as we observe. Grossman et al have published results for water which also show a radial rms distribution flatter than Laufer's. These measurements, which are described in Ref. (35), were obtained with an electromagnetic induction method, and were expressed in terms of the rms of the electric potential gradient, a quantity which, under simplifying assumptions such as the absence of induced currents, etc., was shown to give directly the rms of the velocity field. The fact that the rms of the potential gradient fell below Laufer's rms values for the velocity fluctuations (in agreement with our results) was attributed in Ref. (35) to experimental conditions to which the simplifying assumptions could not be

applied. A definite conclusion is not possible, but the Grossman results do support the possibility that the low rms values and the flatter radial distributions are not entirely due to errors in measurement and data reduction but are caused in part by a characteristic of the flow.

Turning to the data for the 0.5 % Long Lac 17 at the highest Reynolds number ($\mathcal{R}$ = 1.86 x 10^5) we note that, if the trend shown by the existing data were extrapolated toward the wall, the higher than water rms values would correspond to steeper velocity profiles and larger pressure drops than for water. This is contrary to the experimental facts. It is concluded that the true intensities for Long Lac 17 must be lower relative to water as the other Long Lac 17 results show. It appears an experimental error, an odd sample length effect or odd calibration factor may cause the high apparent magnitudes for this particular 0.5 % concentration data.

The Long Lac 17 data in Fig. 11 gives information about concentration and Reynolds number effects on the dimensionless intensities as follows:

1. For the 0.5 % concentration the rms values increase with increase in Reynolds number.

2. The rms values are lower for 0.75 % than for 0.5 % at approximately the same Reynolds numbers.

3. The record for the 0.75 % suspension indicates almost constant turbulence from the centerline to mid-radius. This is in qualitative agreement with the velocity profile for this Reynolds number ($\mathcal{R}$ = 1.57 x 10^5), which shows a plug, or zone of nearly constant velocity over the central region (See Fig. 13).

Turning to Fig. 12 where water, Long Lac 17 and Groundwood are compared as regards the change in rms intensities relative to the value at the centerline, it is seen:

1. Groundwood shows an appreciably flatter distribution than water or Long Lac 17. This is not in agreement with the results of velocity measurements (which, as later figures show, indicate little difference between the velocity profiles of water and Groundwood, especially for low concentrations).

2. For the water rms, there is no meaningful trend of the radial distribution with Reynold's number, the line for the high Reynolds number ($\mathcal{R}$ = 1.79 x 10^5) falling between the lines for the low and intermediate Reynolds numbers. The spread between the relative rms distributions for water gives then an indication of the accuracy to be attributed to the results of the turbulent measurements (the combined accuracy of the turbulent records and of the autocorrelation procedure).

(b) Evidence from Energy Spectra. The energy spectra given in Figs. 7 through 9 indicate the following:

1. The energy spectral density function for water plotted versus cps is similar to the same function for air plotted versus wave number as reported by Laufer (12).

2. At low frequencies up to about 50 cps water and Poplar Groundwood have roughly similar energy distribution.

3. Long Lac 17 compared to water shows lower energy in the 40-60 cps range and higher in the 10-30 cps range.

4. For a given suspension the energy increases from the centerline to the wall.

Item 1 is a qualitative verification that the general trends of the spectra measurements are in agreement with results of others.

The agreement between water and Groundwood at low frequencies suggests that these two would give similar rms intensities except for the anomalous energy hump at 150 cps for the Groundwood. As already noted, the velocity profiles agree which should indicate similar turbulence and momentum transfer processes. It is believed the extra energy at 150 cps is not due to turbulence but to a resonance phenomena as previously discussed. The main effect of turbulence apparently is concentrated in the low frequency range.

Comparing the Long Lac 17 and water, the shift of energy from high to lower frequencies is consistent with a damping of the high frequency small scale turbulence which fiber additions should do.

The energy increases towards the wall is in accordance with the observed increase in apparent rms as the wall is approached.

(c) Summary of Conclusions from Intensity and Energy Distributions. In summary the apparent intensities derived from the correlograms and energy spectra have led to the following conclusions in comparing the fiber suspensions with the newtonian behavior of water:

1. For a given suspension the apparent dimensionless rms increases with $\mathcal{R}$.

2. For a given suspension and Reynolds number the apparent rms increases from the centerline towards the pipe wall.

3. For a given pulp and Reynolds number the apparent rms decreases as the concentration increases.

4. The short fine fibers of Poplar Groundwood show little effect on the turbulence compared to equivalent flows of water.

5. Long Lac 17, on the other hand, definitely affects the turbulent mixing process, damping the higher frequency smaller scale fluctuations to give lower intensities relative to water.

Since the rms is a measure of the total energy of the u'-turbulence, conclusions 1 to 3 apply to total energy as well.

The energy spectrum gives the distribution of the kinetic energy present in the turbulent fluctuations. This energy is supplied by the main flow, and is continuously dissipated by the viscous (molecular) attrition arising from the relative motion of cleavage surfaces within the fluid. Clearly, the greater the area involved in the friction process, i.e., the more subdivided is the flow in small fluid masses, the more effective is the energy dissipation. The concentration of the bulk of the kinetic energy of the Long Lac 17 suspensions at lower frequencies, or within larger size eddies, than for water, must result in what could be termed, using a physiological analogy, a lower metabolism for the suspension. Energy is dissipated at a lower rate, and this is confirmed by the friction loss measurements.

At the 0.50 % concentration, there are not enough fibers in the flow to form extensive entanglements, so that the changes in the power spectrum can describe adequately enough the effect of the addition of fibers to the suspending phase. As the concentration increases, the formation of fiber networks (albeit possibly on a statistical basis only), becomes a progressively more important factor in the energy dissipation and momentum transfer processes. Even though the energy stored in the flow (and hence dissipated), becomes less (as intimated already at the 0.50 % concentration by the lower ordinates of the power spectrum at the centerline, where some form of fiber aggregation is likely to have occurred), the momentum transfer is enhanced by direct fiber to fiber contact. As discussed more extensively in the next sections, this results in blunter velocity profiles than for water, rather than in the sharper ones which could be expected from the consideration of the turbulent energies only.

The cause for the concentration of turbulent energy within lower frequencies, or larger eddy sizes, when fibers are added to the flow, is certainly complex. The following mechanism is proposed to describe the process in qualitative terms. Each fiber or fiber cluster can be considered to form, ideally, the skeleton or the cage of an eddy, entrained by viscous drag. The size of the eddy is determined by the fiber's characteristics; thus larger eddies are associated with the longer and more flexible Long Lac 17 fibers, than with the shorter Groundwood fibers. In a certain sense, the fibers act as a filter, reducing the number of high-frequency, small-scale fluctuations. A comparatively smaller surface area within the fluid is then exposed to viscous dissipation, and, as discussed above, comparatively lower energy losses ensue, than in the absence of fibers.

4. Mean-velocity Measurements

This section, and the following ones, are devoted to the characteristics of the turbulent regime of the suspensions, as they emerge from the analysis of mean-velocity measurements. The mean-velocity profile is determined by the strength of the momentum transfer process. A strong momentum transfer results in nearly equal velocities across the flow, while a weak transfer makes large velocity differentials possible. In the turbulent flow of dilute fiber suspensions, as proposed in our previous report (29), momentum is transferred by two agents: turbulent agitation and fiber - fiber contacts. The wider range of variables in the present experiments enables us to reach a clearer understanding of the part played by flow rate (Reynolds number), concentration and fiber type in determining the strength and relative importance of the two agents. To this aim, we must compare the characteristics of the local turbulence discussed in the previous sections with the overall characteristics of the momentum transfer process, which we begin investigating here; the differences give a measure of the influence of the fiber interaction process.

The mean-velocity profiles for the different suspensions investigated, as well as for water, are plotted adimensionally in Figs. 13-15. Let us examine in detail the effects of different flow rates, concentrations and fiber types. For reasons of convenience in comparing our results with those of other investigators, we shall continue to express flow rates in terms of a conventional Reynolds number based on the viscosity of water. We summarize as follows:

Reynolds Number Effect (Fig. 13)

1. For water, as the Reynolds number increases the velocity profiles become blunter.

2. For the suspensions of a given type and concentration, as the Reynolds number increases the velocity profiles become sharper. The only exception occurs with 0.50 % Long Lac 17, for which the profile is blunter at $\mathbb{R} = 2.24 \times 10^5$ than at $\mathbb{R} = 1.55 \times 10^5$. The effect is particularly marked at the higher concentrations, and for concentrations up to 0.75 % is more marked with Long Lac 17 than with Poplar Groundwood.

Concentration Effect (Fig. 14)

1. For a given fiber and Reynolds number, the velocity profiles become blunter as the concentration increases. Exceptions occur with 1.0 % Groundwood at $\mathbb{R} = 2.26 \times 10^5$ (probably not a very reliable run, as air was observed to be entrained by the suspension), and with the Long Lac 17 runs at the highest Reynolds numbers (the

runs at 0.75 % concentration being also probably effected by air entrainment, which could not be eliminated entirely at high flow rates and concentrations).

2. The previous effect is particularly marked at the lower Reynolds numbers.

Fiber Type Effect (Fig. 15)

1. For a given concentration and Reynolds number, the velocity profiles are blunter for Long Lac 17 than for Groundwood (the only exception is the portion near the wall of the 0.75 % Long Lac 17 profile at $\mathcal{R} = 2.02 \times 10^5$, which as said above, was probably not entirely satisfactory).

The concentration effect was shown by the turbulence and velocity profile measurements reported in Ref. (29). The other two effects which had been inferred from the results of friction loss measurements, are now directly confirmed by the velocity profiles. Thus, we now have ampler evidence to support an interpretation of the turbulent flow mechanism of the suspensions, which was tentatively proposed in the previous report. Further supporting elements will emerge from the analysis of the turbulent data in the following sections. We restate our view of the mechanism as follows:

In the suspensions the fibers cluster. Each cluster has a tendency to interlock with the neighboring ones. Interlocking opposes the action of the shear stresses, and results in a blunter velocity profile (concentration effect). For a particular concentration, as the flow rate (and hence the magnitude of the shear stresses) increases, the equilibrium between disruptive action of the shear stresses and interlocking shifts more in favor of the shear stresses; the links between fiber clusters are more effectively disrupted, and the velocity profiles become sharper (Reynolds number effect). At the lower concentrations, the links between the clusters are weak, and the velocity distribution is not very different from newtonian; thus, an increase in the shear level can cause no major changes in the velocity profiles.

At the higher concentrations, the links are stronger, and the velocity profiles are blunter than the corresponding newtonian ones (concentration effect). In this case an increase in shear level can cause a much more marked change in the velocity profiles. The progressive weakening of the link resistance leads to velocity distributions tending to those for water. It appears that at sufficiently high shear stresses the flow should become fully newtonian. However, this may be approached only asymptotically.

The blunter velocity profiles of the Long Lac 17 suspensions as compared to those of the Groundwood suspensions at the same Reynolds number and concentration (fiber type effect) are a confirmation of the role played by fiber length and flexibility in the strength of the links between fibers and fiber clusters, as suggested in the previous report. The Long Lac 17 fibers, which are much longer, and more flexible than the Groundwood fibers [Table I] have a more pronounced tendency to interlock. Stronger bonds between fibers or fiber clusters, and hence blunter velocity profiles, result.

5. Momentum Transfer Process from the Velocity Profiles

The proportionality between shear stress τ and rate of deformation $\frac{du}{dy}$ at any point along the radius can be expressed by means of a momentum transfer coefficient ϵ as

$$\tau = \rho \epsilon \frac{du}{dy} \qquad [16]$$

Assuming τ to have a linear distribution along the radius, ϵ is given by

$$\epsilon = \frac{\tau_w(1-y/R)}{\rho \frac{du}{dy}} \qquad [17]$$

For a given wall shear stress τ_w, deviations of ϵ from the corresponding newtonian values indicate changes in the relative efficiency of the momentum transfer process, and result in changes in the shape of the velocity distribution (changes in du/dy). It is thus of great significance, in the present experiment, to obtain the ϵ distributions for the various suspensions and flow rates.

(a) Semi-log Velocity Plots; the von Karman Constant, k. In order to compute the slope du/dy of the velocity profiles, necessary to the computation of ϵ according to Eq. [17], the mean-velocity data have been plotted in the semilogarithmic plots of Fig. 16. The plots, in addition to assisting in the computation of the slopes, are useful in their own right, as a further clarification of the characteristics of the velocity distribution.

It is seen that in general the data through the mid-radius range for both water and the suspensions can be represented by a straight line having the equation

$$u = A + B \ln y \qquad [18]$$

where A and B are constants. Expressing [18] dimensionlessly

$$\frac{u}{\sqrt{\tau_w/\rho}} = C + \frac{1}{k} \ln \frac{\sqrt{\tau_w/\rho}\, y}{\nu} \qquad [17]$$

$$\text{or} \quad k = \frac{\sqrt{\tau_w/\rho}}{B} \qquad [18]$$

where k is von Karman's constant from his similarity theory. The dimensionless slope is 1/k. In Table V are given values of k for the mid-radius range for all the plots in Fig. 16. Near the pipe axis and near the wall there are deviations from the mid-radius slope and k values. In summary, the following

are observed from the plots:

1. For water, only at the lower Reynolds number can a single straight line of Eq. [18] be drawn through the experimental points. At the higher Reynolds numbers there are two deviations from a straight line drawn through the experimental points in the central portion of the radius; a deviation near the wall, characterized by a less steep velocity profile, and attributed to the interference of the wall with the large-sized tip of the impact tube; a deviation near the centerline, also characterized by a less steep velocity profile. This second deviation is appreciable only at the higher Reynolds numbers and involves only a small portion of the velocity profile, near the centerline; it is not believed to be caused by instrumental factors.

2. For the suspensions also, the slope of the velocity profile decreases near the center. The phenomenon is more pronounced than for water, particularly at the higher concentrations and with the longer fiber (Long Lac 17), the reduction in slope being larger, and extending over a greater distance from the centerline. The flattening of the slope near the centerline, already evident in Figs. 13-15, is an indication of the strength of the fiber interlocking process. The change in slope near the wall is attributed, as in the water runs, to the interference of the wall with the velocity probe.

3. For the suspensions, the slope of the velocity profiles in the central portion of the radius is not very different from that for water, as shown by Table V (page A-5).

In Table VI the values of k from Table V are rearranged, in order to compare runs with water and different suspensions at approximately the same Reynolds number. Although the Table covers only a limited range of conditions and the values in it have fluctuations which are probably of a statistical nature, it is believed to offer some further insight into the effect of the fibers on the velocity profiles.

Higher values of k correspond to milder slopes in the semi-log diagrams, and hence to a more efficient momentum transfer across the cross-section; this can be caused either by an increase in the strength of the turbulent momentum exchange process, or by the interaction of fibers or fiber clusters. Lower values of k have the opposite significance; a less efficient momentum transfer can be due to damping of turbulence by the fibers, a damping outweighing the tendency to more effective momentum transfer introduced by the presence of the fibers.

Table VI shows that at the 0.50 % concentration the k for Long Lac 17 is low at low Reynolds numbers, and increases with $\mathbb{R}$, reaching approximately the same value as for water at the highest $\mathbb{R}$. This indicates a damping of the momentum exchange processes at the low $\mathbb{R}$'s; the damping becomes progressively less appreciable as $\mathbb{R}$ increases, i.e., as the shear stresses more and more effectively generate turbulence against the stabilizing influence of the fibers. Similarly at the 0.75 % concentration k increases

with $\mathcal{R}$; the final value of 0.34 at $\mathcal{R} = 2.02 \times 10^5$ is higher than for water, but it is difficult to attribute significance to such a difference. The equality of the k values for 0.50 % Long Lac 17 at the low $\mathcal{R}$ (1.08×10^5) and for 0.75 % Long Lac 17 at the intermediate $\mathcal{R}$ suggests the hypothesis of a dependancy of k on shear level and concentration represented by curves with a concavity toward the abscissas, as shown by the curves in Fig. 17. This will be discussed further below.

The k values for Groundwood appear to be either higher than or approximately equal to those for water, so that the trend observed for Long Lac 17 is reversed. However, except for the 1.0 % concentration at the intermediate $\mathcal{R}$, the difference from the water values is not very appreciable. If a significance is attributed to the trend shown by Table VI it would indicate that at low Reynolds numbers the presence of the fibers, rather than damping turbulence, enhances the momentum transfer process. As $\mathcal{R}$ increases, the shear stresses disrupt the fiber associations, and the efficiency of the momentum transfer becomes comparatively lower, approaching that for water.

We could then summarize the nature of the turbulent process for the central portion of the radius in terms of the three main factors which appear to govern it, by means of the functional relationship

$$k = k\left(\mathcal{R}, c, \frac{\ell}{D}\right) \qquad [21]$$

where c is the concentration, ℓ the fiber length and D the pipe diameter.

The first factor is the strength of the turbulent agitations (curve $k_{\mathcal{R}}$ in Fig. 17). The proposed shape of the $k_{\mathcal{R}}$ curve takes into consideration two effects: momentum transfer due to fiber association, and momentum transfer due to turbulent agitation. The first effect is prevalent at low turbulent intensities, i.e., near the origin of the curve, and is characterized by high values of k. As the Reynolds number increases k decreases from the original high values as fiber interlocking is interrupted. Ultimately the turbulent agitation becomes so strong that the trend is reversed and k increases again. At very high shear stresses, it can be expected that the fiber clusters are completely disrupted, and turbulence is damped only through the interaction of the individual fibers with the suspending fluid, rather than through the much stronger interaction which would occur if the fibers were associated in clusters.

The second factor is the concentration of the suspension; it is indicated by the curve k_c proposed in Fig. 17. At low concentrations, the fibers dampen turbulence, and k is low. As concentration increases, the damping becomes more pronounced, but a concentration is rapidly reached at which the damping is offset by the increase in momentum transferred directly by the fibers, so that k reverses its trend and increases. The effect of concentration on k is also a function of the fiber characteristics: different fibers have different effectiveness in damping turbulence and in transferring momentum through their interlocking. This results in different $k_{\mathcal{R}}$ and k_c curves for different fiber lengths (different $\frac{\ell}{D}$). Thus the data for the Groundwood fibers in Table VI would indicate that with shorter fibers;

1) the minimum in the k_c curve occurs at a higher concentration

2) lower shear stresses are necessary for disrupting the association of the shorter fibers, so that the $k_{\mathcal{R}}$ curve is shifted to the left.

It is to be noted that, as a limiting case, for suspensions of rigid materials such as sand grains, k would not be affected by interlocking effects; thus the ordinates of the k_c curves would decrease with concentration (greater concentration causing greater damping), and, for a given concentration, the variation of k with $\mathcal{R}$ would be very minor as compared to the case of the fibers, if present at all. This is in agreement with the findings of Ismail (32) and Vanoni and Nomicos (33).

The previous considerations have been based only on the values of k for the central portion of the radius. As we move toward the centerline, the average shear stresses decrease and turbulence weakens, becoming less effective in disrupting the fiber associations. This would be the equivalent, in Fig. 17, of moving along the $k_{\mathcal{R}}$ curve, toward the origin. Thus, on account of the proposed shape of the $k_{\mathcal{R}}$ curve, near the centerline the k value becomes quite large and the velocity profiles tend to flatten.

(b) Overall Momentum Transfer Coefficients, ϵ. The momentum transfer coefficients ϵ have been computed from Eq. [17], in which du/dy is obtained from the Eq. [18] of the straight lines connecting the experimental points in Fig. 16. The resulting ϵ values are shown in Fig. 18. The ϵ curves

are, of course, only a different way of expressing the strength of the momentum transfer process, which was discussed previously with reference to the trends of the coefficient k. We can summarize the information offered by the curves as follows:

1. For the Groundwood suspensions, the radial distribution of the momentum transfer coefficients is not very different from that for water at approximately the same Reynolds numbers. In particular:

   a. At the low Reynolds numbers ($\mathcal{R} \simeq 1 \times 10^5$) the ϵ values are practically identical with those for water.

   b. At the higher Reynolds number, the distribution is usually skewed, the peak being moved closer to the wall.

   c. The ϵ values for the 1.0 % concentration show the greater variation from the corresponding one for water, and contrary to the trend observed at the lower concentrations, the ϵ values are higher at the intermediate Reynolds number than at the highest Reynolds number, except near the boundary.

   d. For the same Reynolds number, the ϵ values for the 0.50 % and 0.75 % concentrations do not differ very much; the values for the 1.0 % concentration differ instead appreciably.

   e. As observed previously, the results for 1.0 % Groundwood at $\mathcal{R} = 2.26 \times 10^5$ are not entirely reliable, on account of air entrained by the suspension.

2. For the Long Lac 17 suspensions, at the higher concentrations or at the lower Reynolds numbers, the ϵ distribution differs entirely from that for water, changing from parabolic to approximately hyperbolic, with a vertical asymptote in correspondence of the radius of the plug. For a given Reynolds number, as the concentration increases the asymptote moves closer to the wall. In particular:

   a. For the 0.50 % concentration, at the highest and intermediate Reynolds numbers the distribution is parabolic and the ϵ values are very close to the corresponding ones for water; at the lower Reynolds number the distribution is hyperbolic.

   b. For the 0.75 % concentration, the distribution is already hyperbolic at the intermediate Reynolds number. At the highest Reynolds number it is parabolic from the wall to the half-radius (but with much lower ϵ values than the corresponding ones for water); it is hyperbolic from the mid-radius toward the centerline.

   c. At 1.0 % concentration (for which data are available only for the intermediate Reynolds number) the ϵ values increase from the boundary toward the centerline more steeply than the corresponding ones for the lower concentrations.

   d. Near the wall, the ϵ values tend to become appreciably lower than the corresponding ones for water, as concentration increases.

3. For the same concentration and approximately the same Reynolds number, the ϵ values for Long Lac 17 are lower than for Groundwood near the wall, and higher near the centerline. This influence of the fiber characteristics on the efficiency of the momentum transfer process was already pointed out in the discussion of the von Karman coefficients k, but it is more clearly brought to light by the ϵ diagrams. Since, in all cases, near the wall the ϵ values for the suspensions are lower than for water, it is obvious that the turbulent intensities cannot have been higher than for water; this consideration has helped us in Section IV-2c in reaching a conclusion about the reliability of the turbulent measurements in Groundwood and the applicability of a calibration factor to obtain rms values of the turbulent fluctuations from the autocorrelation curves. Near the wall, where fiber interlocking is believed to be less effective and momentum is believed to be transferred primarily by turbulence proper, the low ϵ values for Long Lac 17 with respect to water are in agreement with the turbulent intensities plotted in Fig. (11). Since the turbulent intensities decrease from the wall toward the centerline (Fig. 11) while the overall momentum transfer coefficients increase (Fig. 18) it must be concluded, as already pointed out in our previous report, that:

a. For Long Lac 17 in the range of concentrations observed, the fiber-to-fiber momentum transfer component increases from the wall toward the centerline.

Furthermore, the wider range of variables studied in the present experiments leads us to the following additional conclusions:

b. The fiber-to-fiber momentum transfer component decreases in importance with Reynolds number; at very high Reynolds numbers it may practically disappear (e.g., see ϵ curves for 0.50 % Long Lac 17 in Fig. 18).

c. The fiber-to-fiber momentum transfer components of other fiber suspensions give an indication (from measurements of friction losses, velocity profiles and turbulent intensities) to follow basically the same trends as in the Long Lac 17 suspensions. With shorter fibers, as evidenced by the experimental data for Groundwood, the fiber-to-fiber momentum transfer phenomena are - other things being equal - less marked, the distribution of the overall momentum transfer coefficient remaining approximately parabolic up to higher concentrations tested. With longer fibers the fiber-to-fiber momentum transfer components are believed to be enhanced, so that the departure from the parabolic ϵ distribution is believed to occur at lower concentrations - and to remain at higher flow rates - than observed in the Long Lac 17 suspension.

4. Finally, the relative magnitude of the ϵ values near the wall, for water and the suspensions, is in close agreement with the results of friction loss measurements, which show lower friction factors for the suspensions than for water, the difference being more marked for the Long Lac 17 than for the Groundwood suspensions. It is particularly noteworthy, how the small difference in f values for 0.50 % and 0.75 % Groundwood (as compared to the f values for 1.0 % Groundwood) is in agreement with what was observed for the ϵ values in point 1d above.

V. SUMMARY OF CONCLUSIONS AND RECOMMENDATIONS

In the present investigation, turbulent fluctuations and velocity distributions have been measured in water and in suspensions of long and short papermaking fibers (Long Lac 17 and Poplar Groundwood respectively). The experiments extend the range of variables covered in a previous report [Ref. (29)], and confirm and extend the conclusions regarding the mechanism of turbulence and the momentum transfer process in dilute fiber suspensions.

The significant findings from the correlograms, energy spectra and velocity profiles can be summarized as follows:

1. The apparent dimensionless rms turbulence intensities increase as Reynolds number increases and decrease as the concentration increases, other things being equal.

2. The apparent intensities increase from the centerline toward the pipe wall, but generally at a lower rate than shown by Laufer.

3. In the suspensions, the velocity profiles become blunter than the corresponding newtonian profiles for water, as concentration and fiber attitude to interlocking increase.

4. For a given concentration and fiber type, the velocity profiles of the suspensions become sharper as the flow rate (Reynolds number) increases, and tend to approach the profiles for water.

5. Energy spectra for water, for a 0.50 % Long Lac 17 suspension and for a 0.50 % Groundwood suspension, at approximately the same Reynolds number ($\sim 1.8 \times 10^5$) indicate that:

   a) the energy distribution for water has the same trend observed by Laufer in air.

   b) for Long Lac 17, the energy is shifted to lower frequencies than for water.

   c) for Poplar Groundwood, the energy distribution is roughly similar to that for water, up to 50 cps.

These results refer to flow conditions (concentration, Reynolds number) at which fiber interactions in the suspensions are believed to be weak, as suggested by the relatively small difference between the velocity profiles for water and the suspensions.

The preceding points confirm the hypothesis that the transmission of shear stresses and the diffusion and mixing depends on the combined roles of turbulence and fiber entanglement. The interpretation is summarized as follows:

6. At a given Reynolds number, the efficiency of the overall momentum transfer process (and hence the value of the momentum transfer coefficient ϵ) increases with concentration, with fiber

length and other parameters determining the fiber attitude to interlocking. At the same time, the increase in concentration and fiber attitude to interlocking dampen the turbulent intensities (point 1), so that the blunter velocity profiles observed in the suspensions, as compared to those for water (point 3), are due to fiber entanglement being more effective than turbulence as a momentum transfer agent.

7. Near the walls, where the presence of a solid boundary hampers fiber interlocking, momentum is believed to be transferred primarily by turbulence. Since turbulence is damped by the fibers, the velocity profile must be less sharp than the corresponding one for water, so that, as experimentally observed, the friction losses for the suspensions are lower than for water at the same Reynolds number.

8. For a given concentration and fiber, an increase in the Reynolds number enhances the effectiveness of turbulence and makes fiber entanglement less important, so that ultimately at high Reynolds numbers the velocity profiles tend to approach those for water, (point 4).

9. The concentration of turbulent energies at lower frequencies for Long Lac 17 as compared to water (point 5b) is interpreted as an indication that small-scale turbulence is damped by fiber additions. The effectiveness with which the small-scale components of the turbulent field are damped appears to be a function of fiber length, (or, more properly, fiber attitude to interlocking), as indicated by the observation that the energy distribution in the suspension of the shorter Groundwood fibers is similar to that in water, (point 5c).

This and the previous TAPPI sponsored investigations at M.I.T. have demonstrated the complexity with which many different factors, each important and operating simultaneously, control turbulent mixing and diffusion in a fiber suspension. The above explanation describes the general mechanism as deduced from the resulting behavior of the fibers tested. This description should serve as a useful guide in design and application. However, the description is general rather than definitive in that it does not isolate adequately the relative importance of the key factors in establishing the balance between the roles of turbulence and fiber entanglement in a given flow situation. This is due, in part, to limitations yet remaining in the experimental and analytical procedures, but more importantly is the consequence of the inherent complexity of the fiber suspensions themselves. It is apparent that a truly satisfactory and effectively useful understanding will require a segregation of the several fiber properties and their individual effects on the flow behavior. To accomplish this it appears from the experience to date that before extending the investigations of fiber suspensions as such, it will be more profitable to consider simpler suspension systems in which one role definitely predominates. It is believed this approach should be undertaken to realize a significant forward step in the unravelling of this problem. Simultaneously, of course, the experimental and anayltical procedures should be perfected.

Consequently, it is recommended that further investigations follow the above course. In particular, for the immediate future it seems especially important to:

1. Consider the basic question of the role played by suspended material in modifying the turbulent field and diffusion and mixing in the absence of any interlocking phenomena. This can be investigated with suspensions of inert materials which cannot entangle, such as rigid particles of simple geometric shapes.

2. Further improve the procedures for experiment and analysis with the objective of better accuracy in quantitative values and the elimination of apparent anomalies between records for different suspensions, including:

   a) Increased frequency response of turbulence gage.

   b) Means for velocity and turbulence probing closer to the boundaries.

   c) Continued investigation of periodicities in correlograms, and the influence of sample time and frequency on the correlogram and hence on the calibration factor for rms magnitudes.

   d) Generally extend the range of flow variables and concentrations for both autocorrelation and energy spectra analysis.

REFERENCES

1. Taylor, G. I. (1935) Statistical Theory of Turbulence. Parts 1-4. Proceedings Royal Soc. A, 151, 421.

2. Taylor, G. I. (1921) Diffusion by Continuous Movements. Proceedings London Math. Soc. 20, 196.

3. Taylor, G. I. (1938) The Spectrum of Turbulence. Proceedings Royal Soc. A, 164, 476.

4. Wiener, N. (1930) Generalized Harmonic Analysis, Vol. 55, p. 117-258.

5. Kolmogoroff, A. (1941) The Local Structure of Turbulence in Incompressible Viscous Flow for very large Reynolds Numbers. Comp. rend., Acad. Sci. URSS, Vol. 30, No. 4, p. 301.

6. Batchelor, G. K. (1947) Kolmogoroffs' Theory of Locally Isotropic Turbulence. Proceedings Cambridge Phil. Soc. Vol. 43, p.553.

7. Heisenberg, W. (1948) Zur Statistichen Theorie der Turbulenz. Zeitschr. Phys., Bd. 124, Heft 7/12 p. 628.

8. Batchelor, G. K. (1956) The Theory of Homogeneous Turbulence, Cambridge University Press.

9. Agostini, L. and Bass, J. (1955) The Theories of Turbulence, NACA TM 1377.

10. Batchelor, G. K. (1948) Recent Developments in Turbulence Research. Introduction,Proceedings Seventh Int. Cong. Appl. Mech. (London) pp. 27-56.

11. Laufer, J. (1951) Investigation of Turbulent Flow in a Two-Dimensional Channel. NACA Rep. 1053. (Superseded [illegible]).

12. Laufer, J. (1955) The Structure of Turbulence in Fully Developed Pipe Flow, NACA Rep. No. 1174.

13. Tchen, C. M. (1953) On the Spectrum of Energy in Turbulent Shear Flows, J. Res.,Nat. Bur. Stand. 50, 51-62.

14. Batchelor, G. K. (1950) Note on Free Turbulent Flows, with Special Reference to the Two-dimensional Wake. Jour. Aero. Sci. Vol. 17, No. 7, p. 441-445.

15. Townsend, A. A. (1956) The Structure of Turbulent Shear Flow, Cambridge University Press.

16. Wiener, N. (1950) Extrapolation, Interpolation and Smoothing of Stationary Time Series; John Wiley and Sons, Inc.

17. Rice, S. O., Mathematical Analysis of Random Noise. The Bell System Tech. Jour., Vol. 23, No. 3, July 1944, p. 282-332; Vol. 24, No. 1, Jan. 1945, p. 46-108.

18. Bendat, J. S. (1958) Principles and Applications of Random Noise Theory, John Wiley and Sons, Inc.

19. Davenport, W. B., Jr., and Root, W. L. (1958), Random Signals and Noise, McGraw-Hill Book Co., Inc.

20. Davenport, W. B., Jr. (1951) Correlator Errors Due to Finite Observation Intervals. Technical Report 191, Research Laboratory of Electronics, M.I.T.

21. Davenport, W. B., Jr., Johnson, R. A., and Middleton, D. (1952) Statistical Errors in the Measurements on Random Time Functions. J. Applied Physics, 4, 377-382.

22. Doob, J. L. (1953) Stochastic Processes. John Wiley and Sons, Inc.

23. Weiss, T. F., (1959) Some Properties of the Finite Time Sample Autocorrelation of the Electroencephalogram, M. S. Thesis in Electrical Engineering M.I.T.

24. Tukey, J. W. (1949) The Sampling Theory of Power Spectrum Estimates. Symposium on Applications of Autocorrelation Analysis to Physical Problems, Woods Hole, Mass. ONR Publication NAVEXOS - P-735.

25. Tukey, J. W., and Hamming, R. W. (1949) Measuring Noise Color 1. Memo MM-49-110-119. Bell Telephone Laboratory.

26. Dryden, H.L. (1943) A Review of the Statistical Theory of Turbulence, Quarterly of Applied Mathematics, Vol. 1, p. 7.

27. Freeman, M. Z., and Frishkopf, L. S. (1958) Notes on Work Done in EEG. Internal memo, Communications Biophysics Laboratory, Research Laboratory of Electronics, M.I.T.

28. Barlow, J. S. and Brown, R. M. (1955) An Analog Correlator System for Brain Potentials. Technical Report 300, Research Laboratory of Electronics, M.I.T.

29. Daily, J. W. and Bugliarello, G. (1958) The Effects of Fibers on Velocity Distribution, Turbulence, and Flow Resistance of Dilute Suspensions. Technical Report No. 30, Hydrodynamics Laboratory, M.I.T.

30. Lin, C. C. (1953) On Talyor's Hypothesis and the Acceleration Terms in the Navier-Stokes Equations. Quant. Applied Math., Vol. X, No. 4, p. 295-306.

31. Roshko, A. (1954) On the Development of Turbulent Wakes from Vortex Sheets, NACA Report No. 1191.

32. Ismail, H. M. Turbulent Transfer Mechanism and Suspended Sediment in Closed Channels. Proceedings, ASCE, Feb. 1951.

33. Vanoni, V. A. and Nomicos, G. N. Resistance Properties of Sediment-Laden Streams. Journal of the Hydraulics Division, Proceedings of the ASCE, May 1959.

34. Blackman, R. B. and Tukey, J. W., The Measurement of Power Spectra. Dover Publications Inc., New York, 1958.

35. Grossman, L. M., Li, H. and Einstein, H. A., Turbulence in Civil Engineering: Investigations in Liquid Shear Flow by Electromagnetic Induction. Journal of the Hydraulics Division, Proceedings of the ASCE, October, 1957.

36. Ippen, A. T., Tankin, R. S. and Raichlen, F., Turbulence Measurements in Free Surface Flow with an Impact Tube-Pressure Transducer Combination. Technical Report No. 20, M.I.T. Hydrodynamics Laboratory.

TABLE I

PRINCIPAL FIBER CHARACTERISTICS

Fiber	Kraft Softwood (Long Lac 17)	Groundwood
Composition	65 °/o spruce, 35 °/o Jack Pine	Poplar
Fiber width, microns (weighted average)	43	40
Fiber length, mm (weighted average)	2.52	0.49
Length to width ratio	58.5	12.2
Hydrodynamic specific surface ($cm^2/cm3$)	9,900	22,000
Hydrodynamic specific volume (cm^3/g)	1.28	2.06
Millions of fibers per gram of pulp	5.28	Very large
Freeness, cm3 S-R	870	500
Ratio pipe diameter (2") to fiber length	20.2	104

TABLE II

TEST CONDITIONS FOR EXPERIMENTS

Concentrations and Approximate Reynolds Numbers

Fluid	Test Reynolds Numbers					
	Velocity Profiles			Turbulence Measurements		
Water	9.6×10^4	1.55×10^5	2.05×10^5	8.7×10^4	1.67×10^5	1.79×10^5
Long Lac 17						
0.5 %	1.08×10^5	1.55×10^5	2.24×10^5	9.55×10^4	1.65×10^5	1.86×10^5
0.75 %		1.55×10^5	2.02×10^5		1.57×10^5	
1.0 %		1.55×10^5				
Poplar Ground Wood						
0.5 %	1.0×10^5		2.26×10^5	1.0×10^5		1.71×10^5
0.75 %	9.4×10^4		1.87×10^5			1.71×10^5
1.0 %		1.67×10^5	2.26×10^5			1.75×10^5

TABLE III

ORDINATES OF AUTOCORRELOGRAMS AT ZERO DELAY TIME

Fluid	$\mathbb{R}$	Sample Length T (sec)	Y_A (ft/sec)^2 x coefficient		
			$y/_{R=0.25}$	$y/_{R=0.50}$	$y/_{R=1.0}$
Water	8.7×10^4	10	67.5	58	31
	1.67×10^5	10	184	158	60
		20	225	175	73
	1.79×10^5	10	133	100	59
		20	233	205	101
0.50 % Long Lac 17	9.55×10^4	10		6.0	
	1.65×10^5	10	79	52	25
		20	79	60	28
	1.86×10^5	20	355	276	98
0.75 % Long Lac 17	1.57×10^5	10	38	12	18
0.50 % Poplar G'wood	1.0×10^5	20	63	52	32.5
	1.71×10^5	20	880	720	485
		20*	720	700	415
		30		920	
		45		1770	
0.75 % Poplar G'wood	1.71×10^5	20	950	990	705
1.0 % Poplar G'wood	1.75×10^5	10			235
		20	640	535	420
		30			550

Note: *: Different run from the previous one; an average value for the two runs has been used in Fig. 12.

TABLE IV

ANALYSIS OF PERIODICITIES IN AUTOCORRELOGRAMS

	$\mathbb{R}$	Sample Length T (sec)	ω_o (cps)			Ω (rps)	Ω_b (cps)	Frequency of Peak in Power Spectra (c
			$y/_R$=0.25	$y/_R$=0.50	$y/_R$=1.0			
	8.7 x 10^4	10	28.6	31.2	31.2	11.2	56	
	1.67 x 10^5	10	26.3	26.3	23.7			
		10	22	23.3	23.3			
		20			45			
	1.79 x 10^5	10	50	50	50			10; 30; 50
		20			45			
17	1.65 x 10^5	10	50	50	50			
		20		50	50			
	1.86 x 10^5	20		56				10; 30
17	1.57 x 10^5	10	40	40	45			
od	1.0 x 10^5	20	151	149	149	11.6	59	
	1.71 x 10^5	20	149	149	149	20.8	104	10; 30; 55; 150
		20	143	143	143			
od	1.71 x 10^5	20	161	161	161	20.8	104	
od	1.71 x 10^5	20	192	192	192			

: frequency of periodicities in autocorrelogram.

: rotating speed of pump.

: frequency of pump rotor vanes passing the volute tongue (cutwater).

TABLE V

EXPERIMENTAL VALUES OF VON KARMAN CONSTANT k

	$\mathbb{R}$	k from Eq. [5]
Water	9.6×10^4	0.29
	1.55×10^5	0.24
	2.05×10^5	0.28
Long Lac 17, 0.50 %	1.08×10^5	0.17
	1.55×10^5	0.26
	2.24×10^5	0.27
Long Lac 17, 0.75 %	1.55×10^5	0.18
	2.02×10^5	0.34
Long Lac 17, 1.0 %	1.55×10^5	0.31
Groundwood, 0.50 %	1.00×10^5	0.30
	2.26×10^5	0.27
Groundwood, 0.75 %	9.4×10^4	0.31
	1.87×10^5	0.26
Groundwood, 1.0 %	1.67×10^5	0.37
	2.26×10^5	0.25

TABLE VI

VON KARMAN CONSTANT k : REARRANGEMENT OF DATA FROM TABLE V

$\mathbb{R}$ (approx.)	Water	Long Lac 17			Groundwood		
		0.50 %	0.75 %	1.0 %	0.50 %	0.75 %	1.0 %
1×10^5	0.29	0.17			0.30	0.31	
1.5×10^5	0.24	0.26	0.18	0. 31			0.37
2×10^5	0.28	0.27	0.34		0.27	0.26	0.25

BLOCK DIAGRAM OF CALIBRATION SETUP

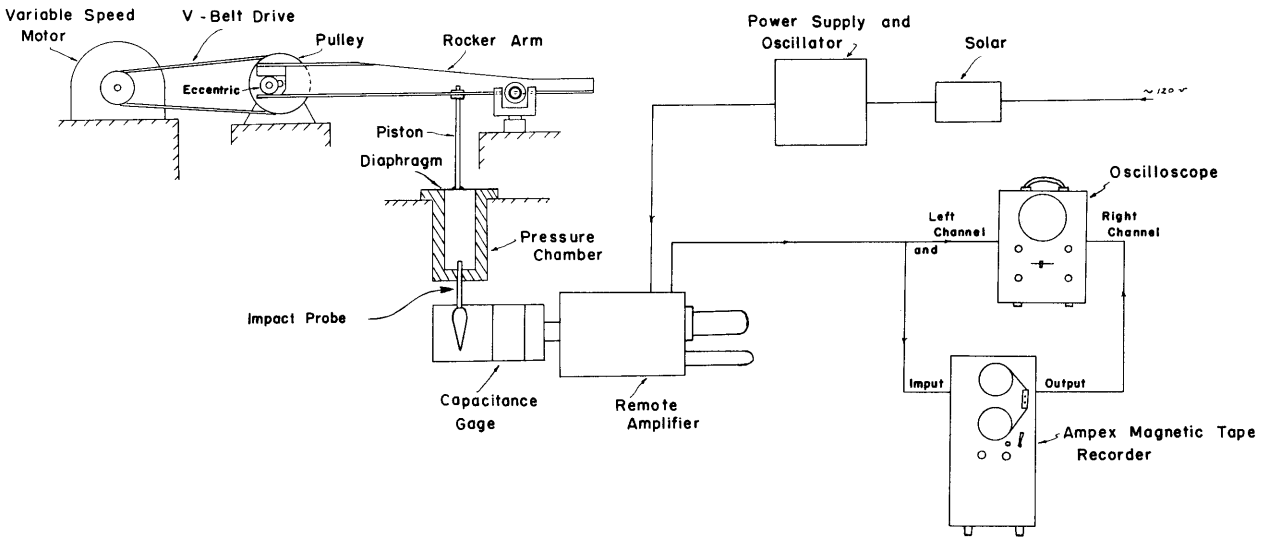

Fig. 1 Block Diagram of Calibration Set-up

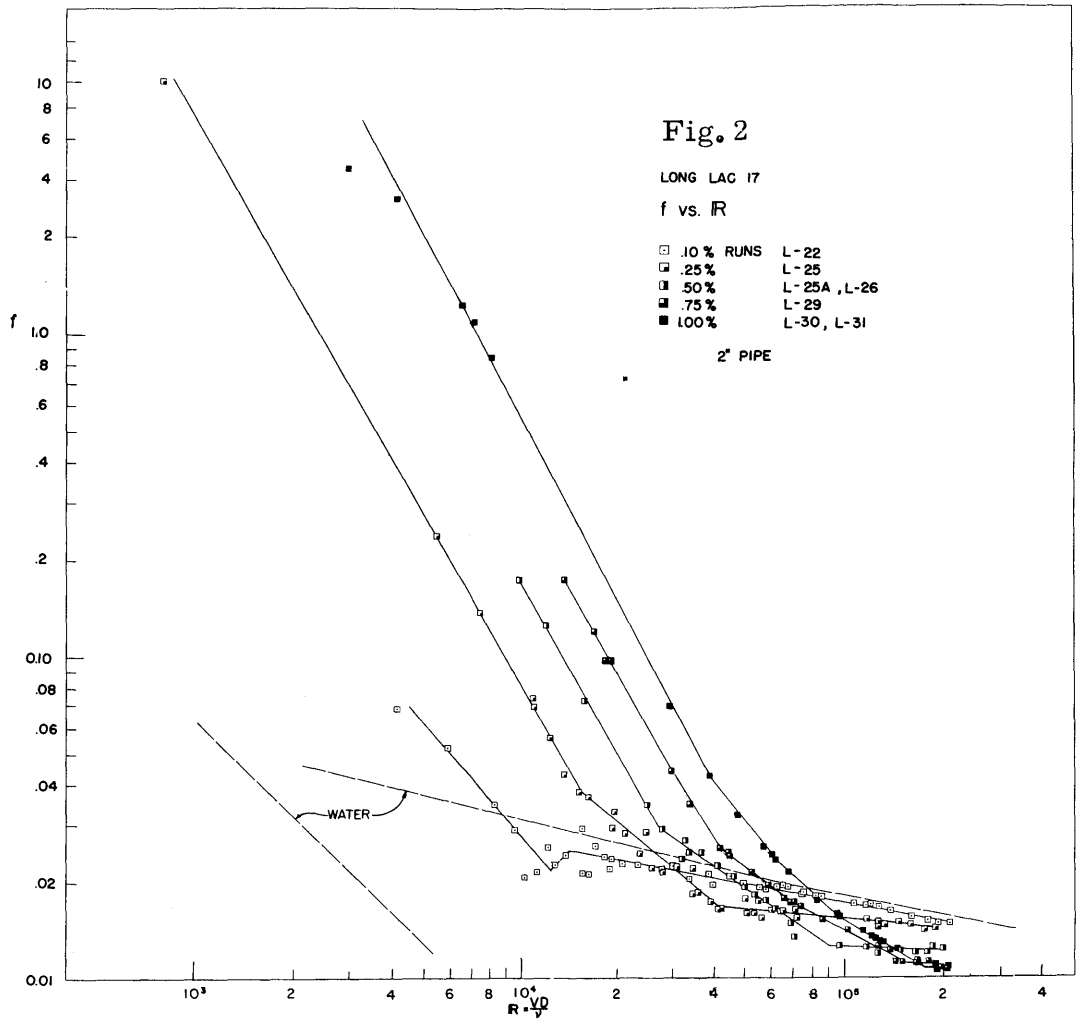
Fig. 2
LONG LAC 17
f vs. R
.10 % RUNS L-22
.25 % L-25
.50 % L-25A , L-26
.75 % L-29
1.00 % L-30, L-31
2" PIPE
f
WATER
R = VD/ν

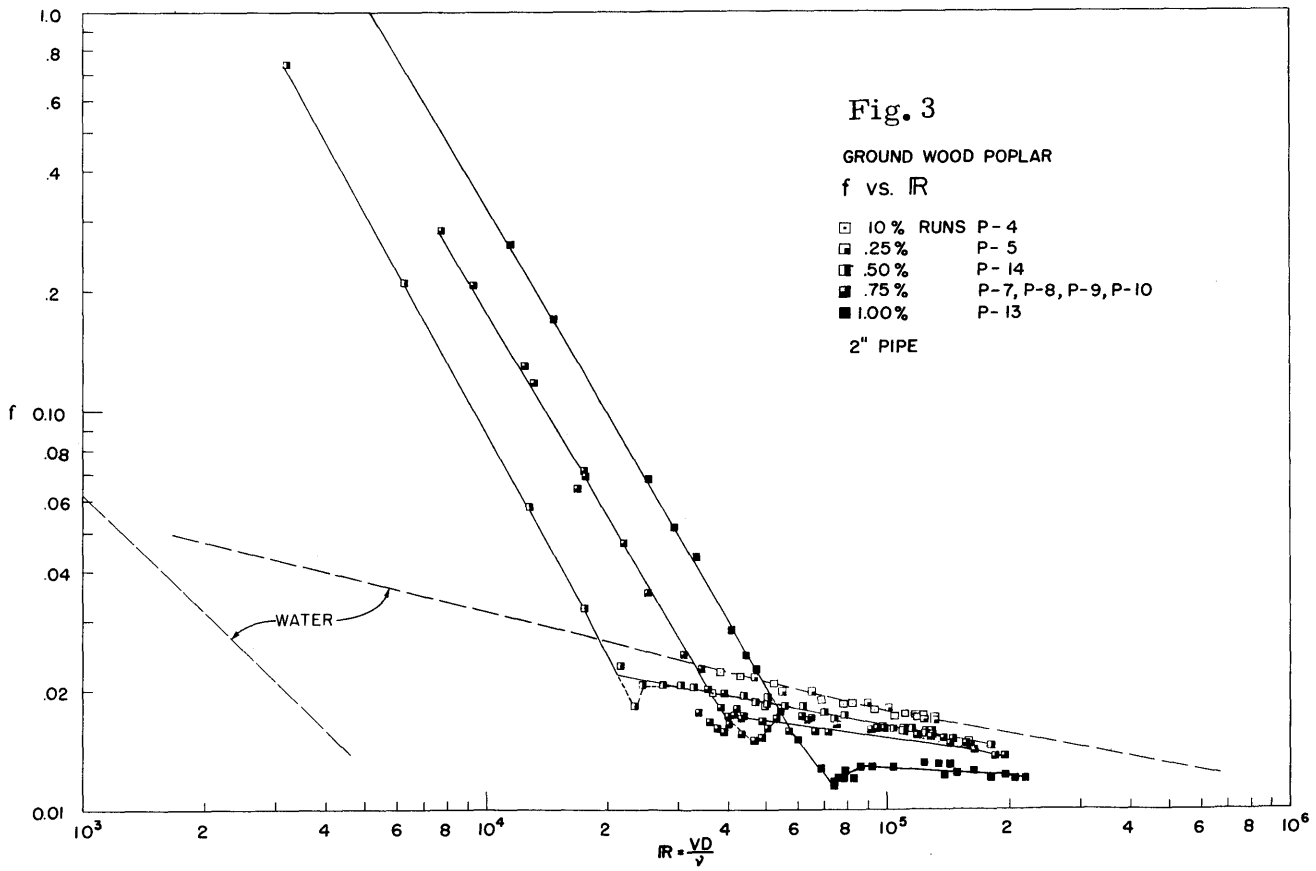
Fig. 3
GROUND WOOD POPLAR
f vs. R
10 % RUNS P-4
.25 % P-5
.50 % P-14
.75 % P-7, P-8, P-9, P-10
1.00 % P-13
2" PIPE
f
WATER
R = VD/ν

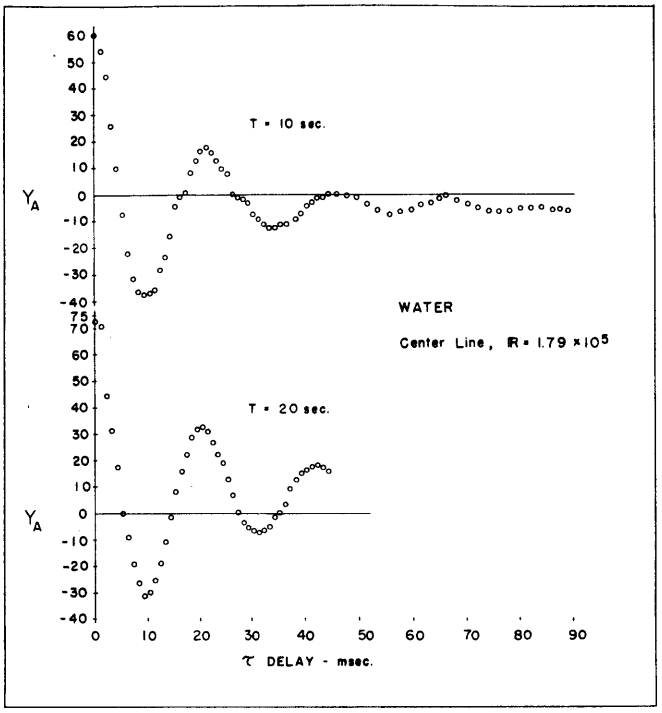

Fig. 4 Autocorrelogram - Water, R = 1.79 x 10^5

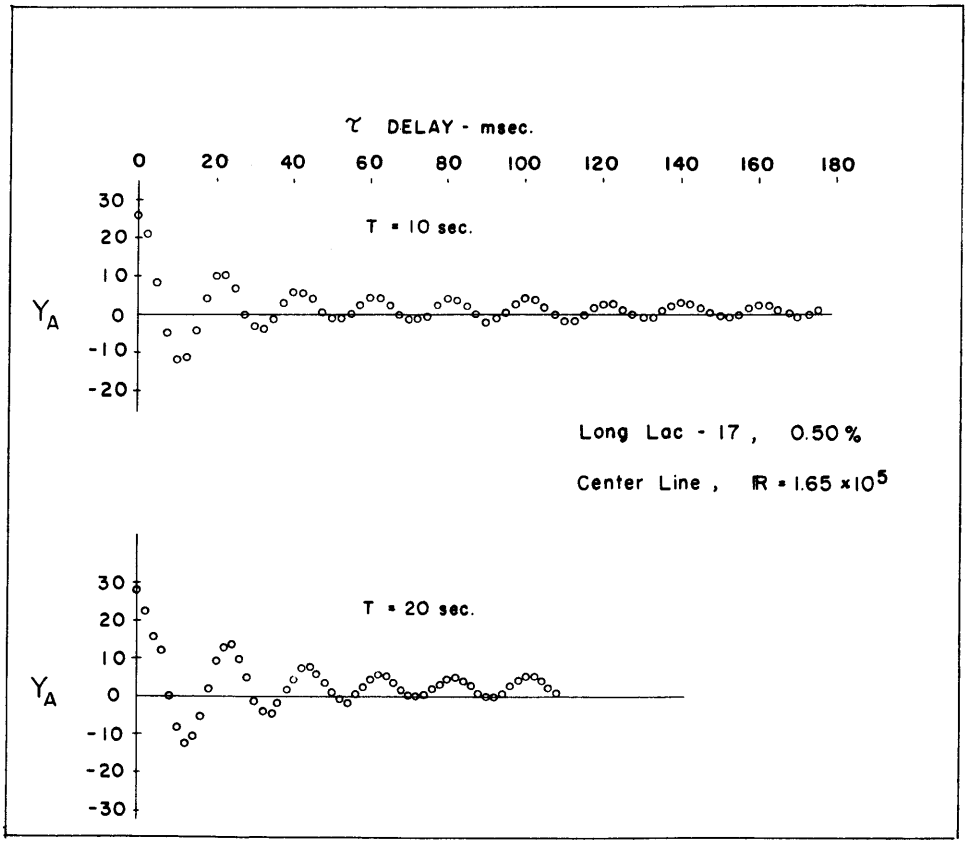

Fig. 5 Autocorrelogram - Long Lac 17, 0.5 °/o, Centerline, R = 1.65 x 10^5

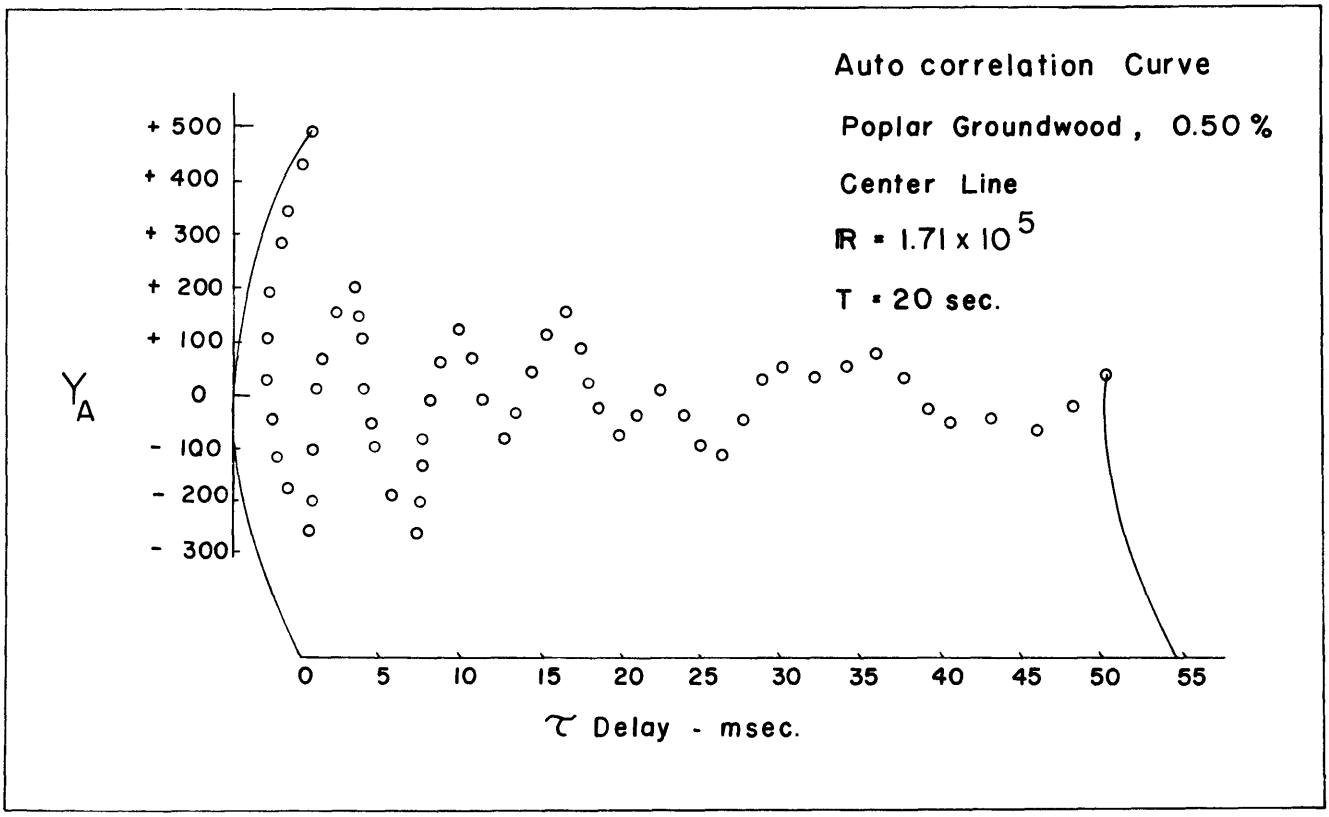

Fig. 6 Autocorrelogram, Popular Groundwood, 0.5 °/o , Centerline, $R = 1.71 \times 10^5$

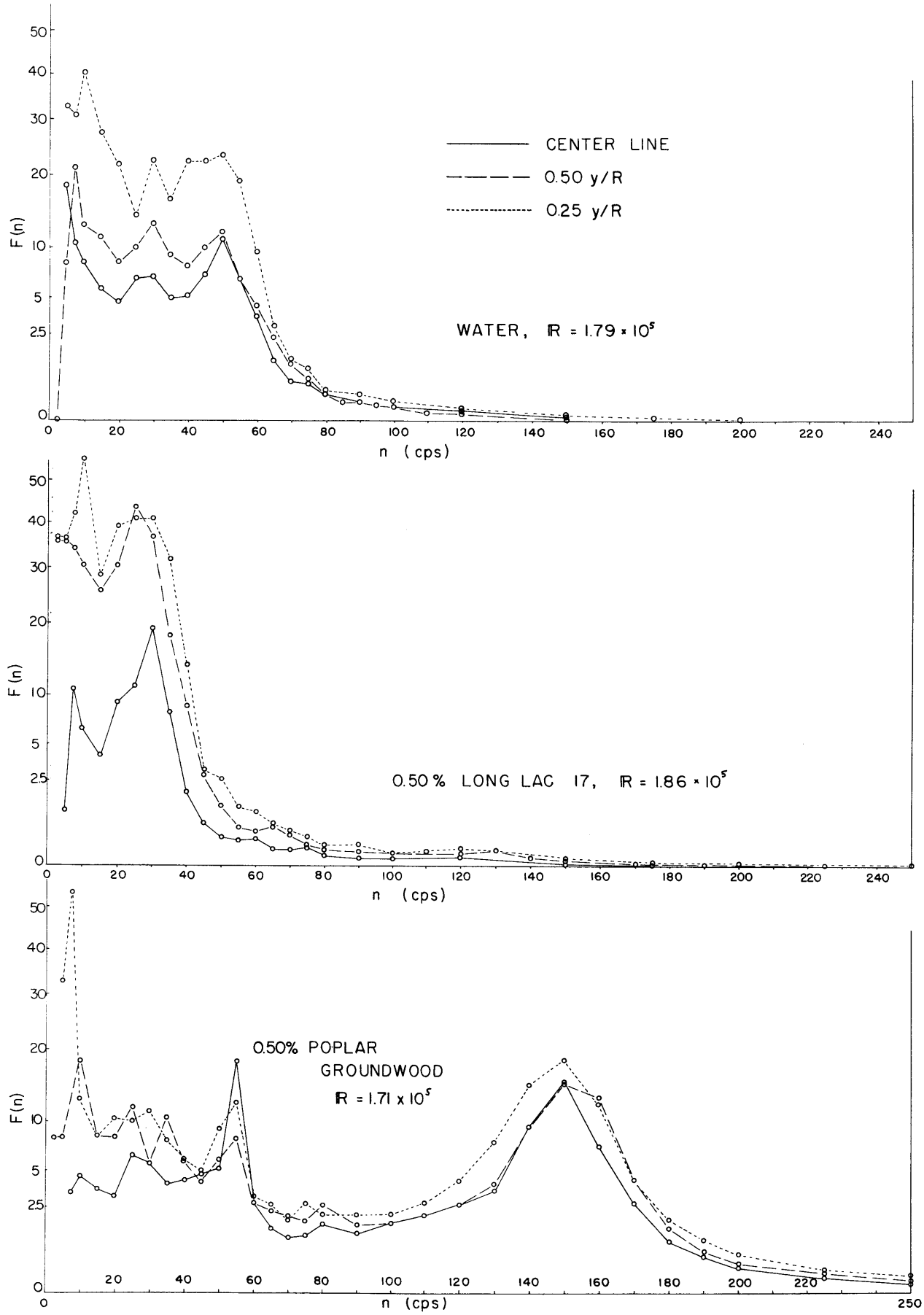

Fig. 7 u'-Energy Spectra .
Ordinate is proportional to mean square intensities per unit mass per cycle per second at a given frequency

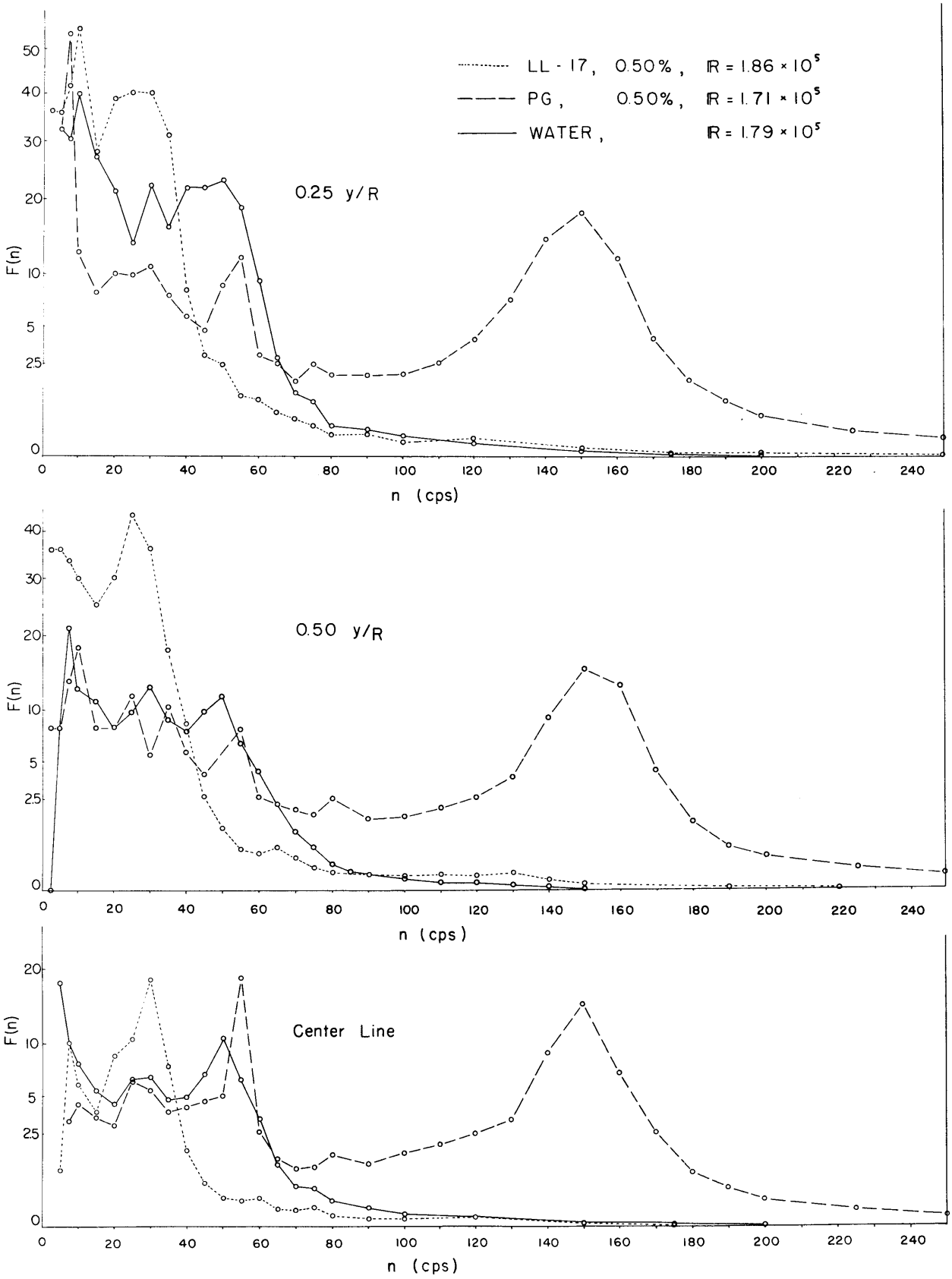

Fig. 8 u'-Energy Spectra - Comparisons at Same Radii.
Ordinate is proportional to mean square intensities
per unit mass per cycle per second at a given frequency

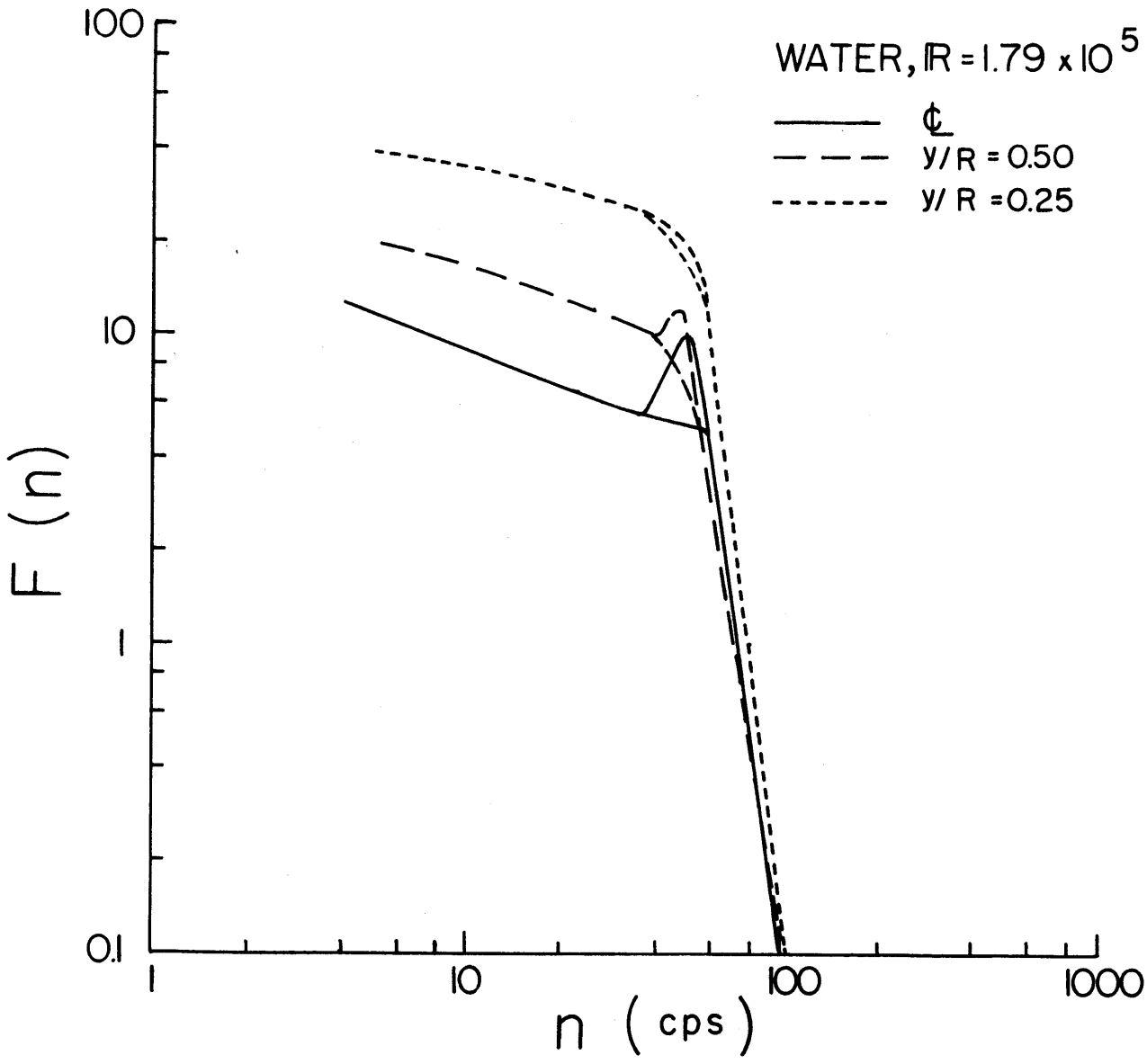

Fig. 9 u'-Energy Spectra for Water (log-log scale)

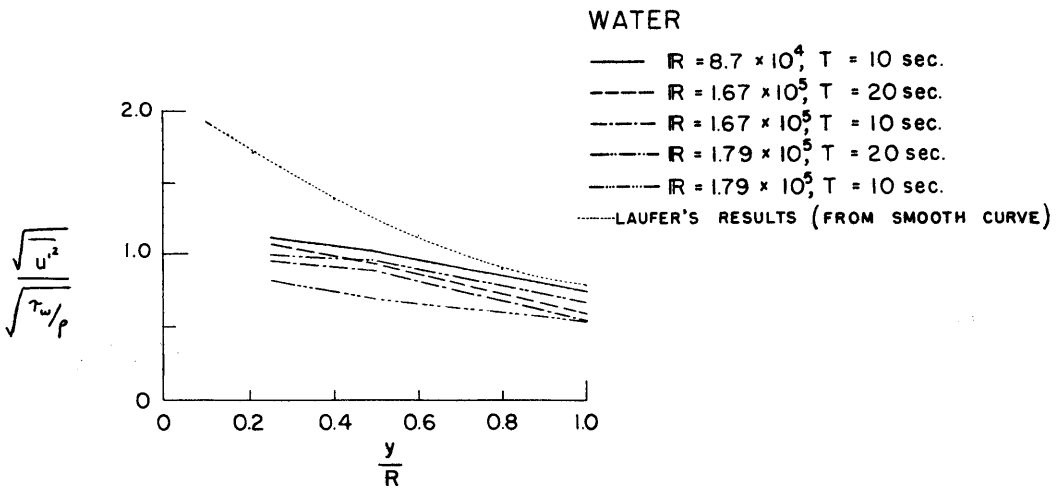

Fig. 10 u'-Turbulence Intensities - Water

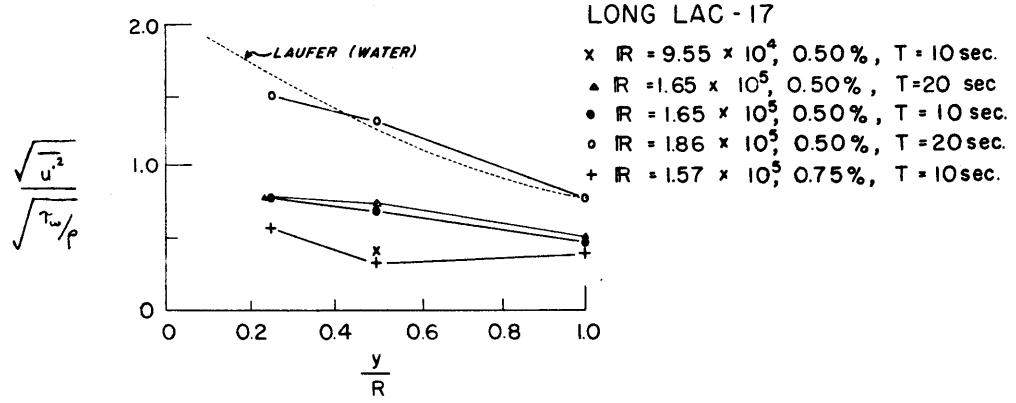

Fig. 11 u'-Turbulence Intensities - Long Lac 17

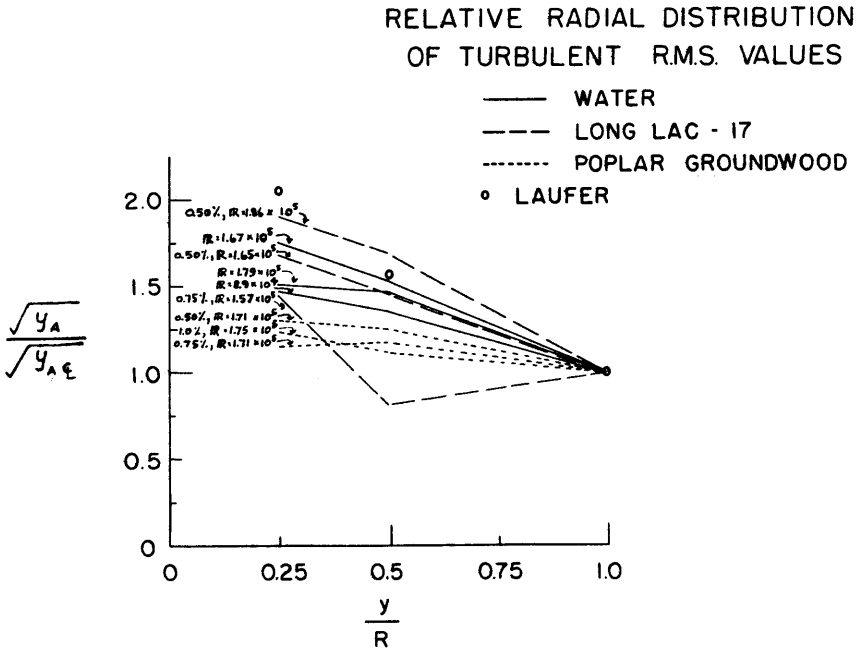

Fig. 12 Relative Radial Distribution of u'-Turbulence

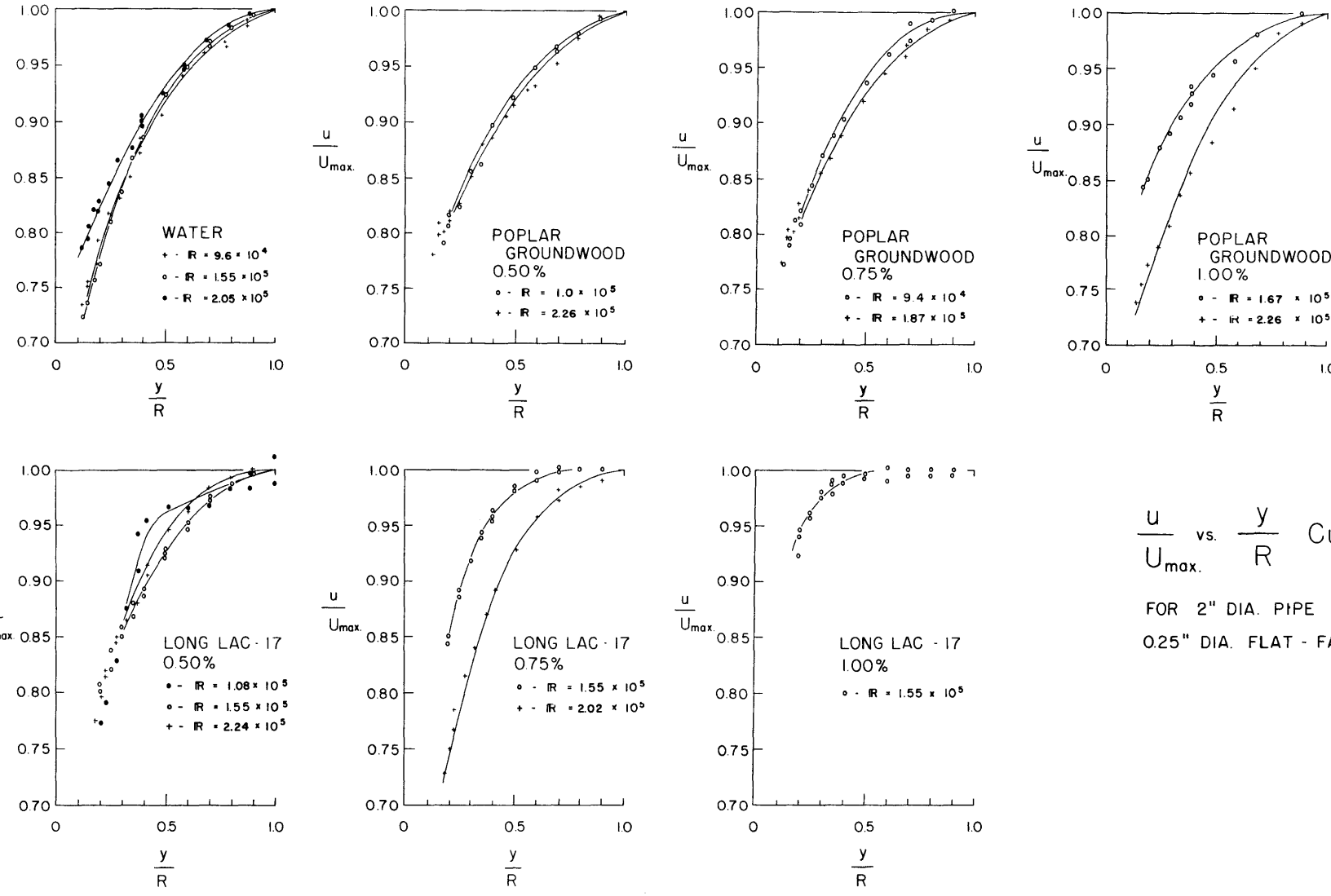

$\frac{u}{U_{max.}}$ vs. $\frac{y}{R}$ C

FOR 2" DIA. PIPE

0.25" DIA. FLAT - F

Fig. 13 Dimensionless Mean-Velocity Profiles

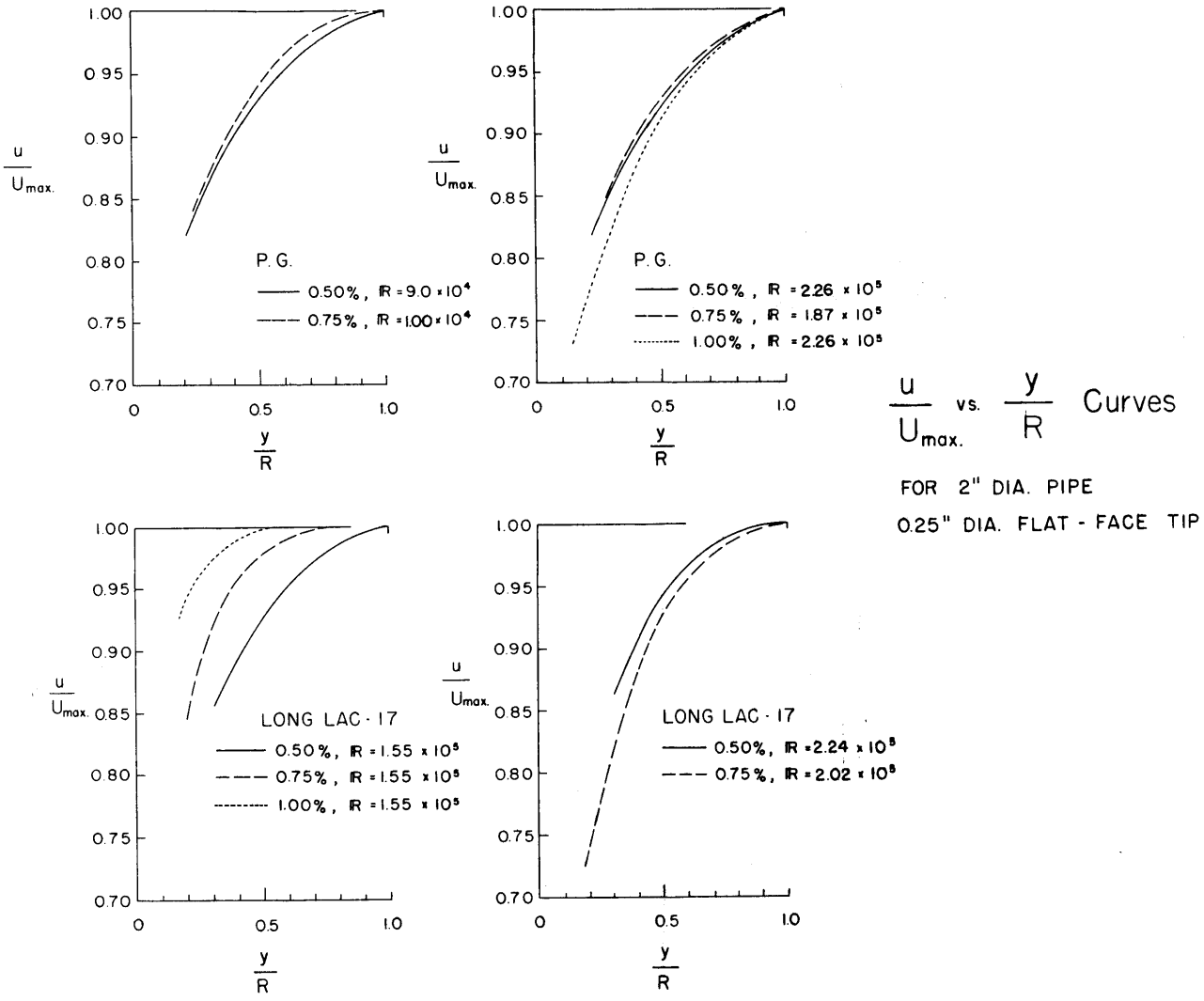

Fig. 14 Dimensionless Mean-Velocity Profiles - Comparisons at approximately constant Reynolds Number

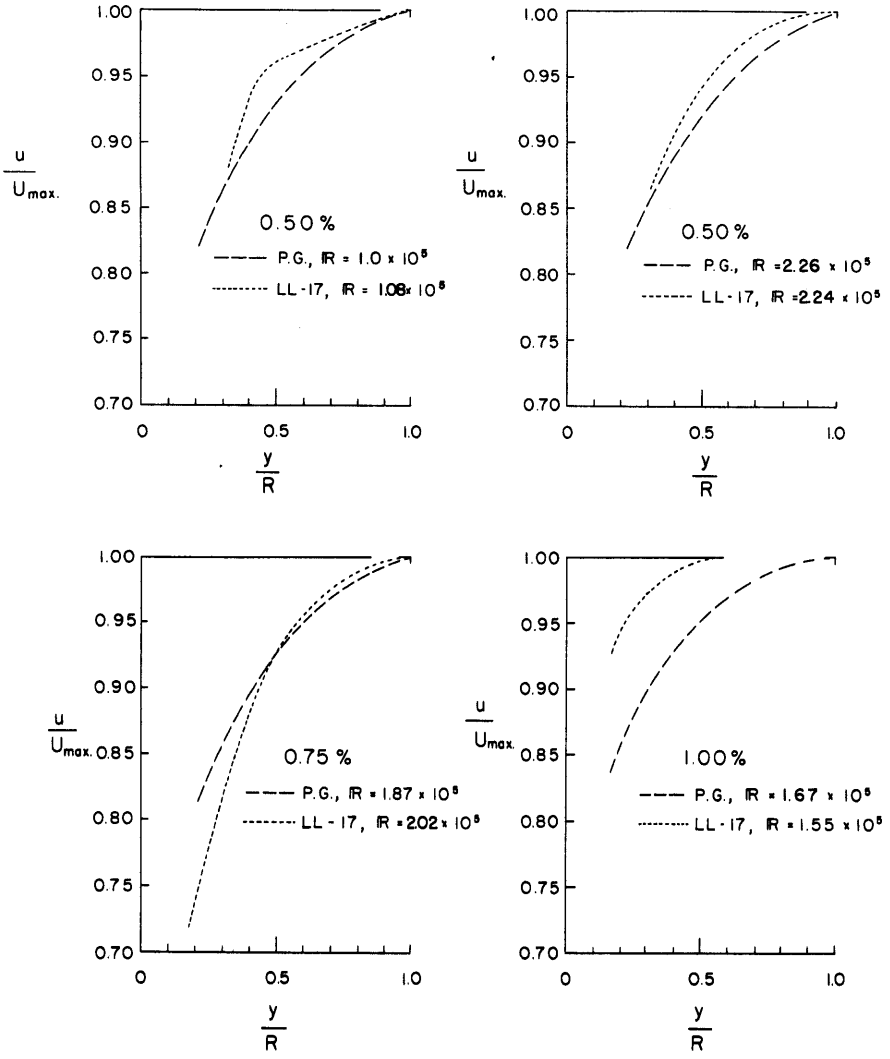

$\frac{u}{U_{max.}}$ vs. $\frac{y}{R}$ Curves

FOR 2" DIA. PIPE

0.25" DIA. FLAT - FACE TIP

Fig. 15 Dimensionless Mean-Velocity Profiles - Comparisons at constant concentration

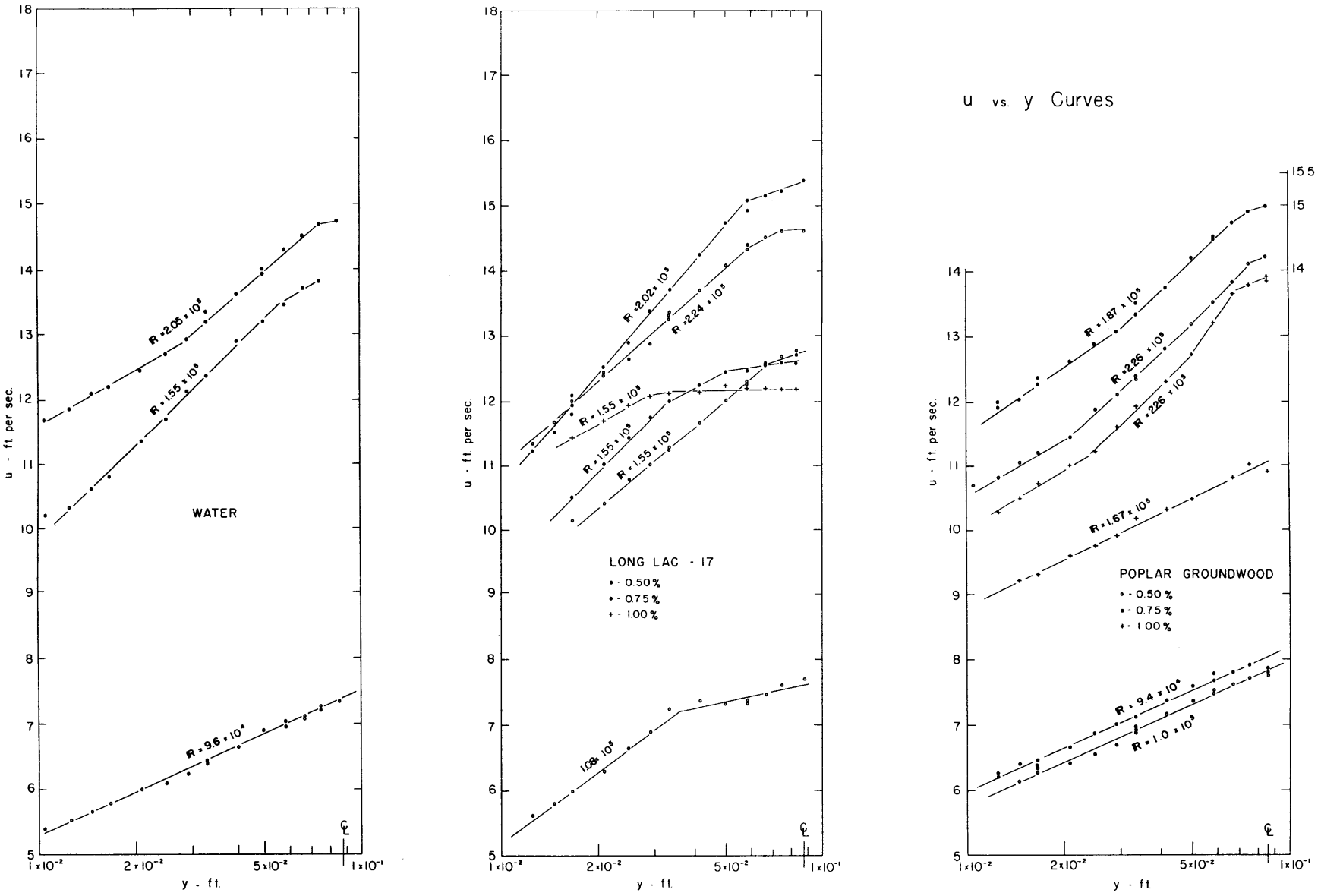

Fig. 16 Velocity Profiles - Semi-log Plot

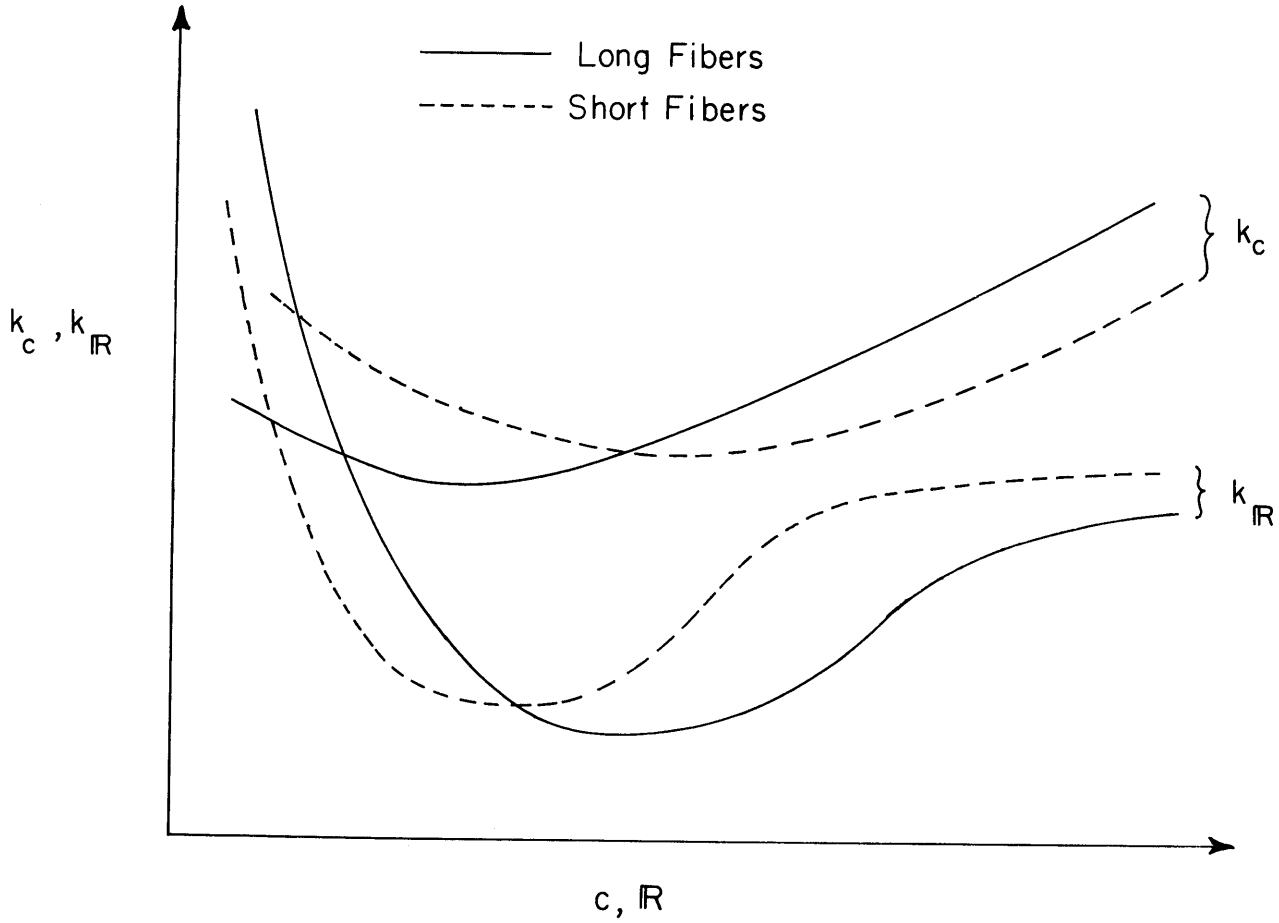

Fig. 17 Schematic Representation for Hypothesis of Influence of Reynolds Number, Concentration, Fiber Length on k

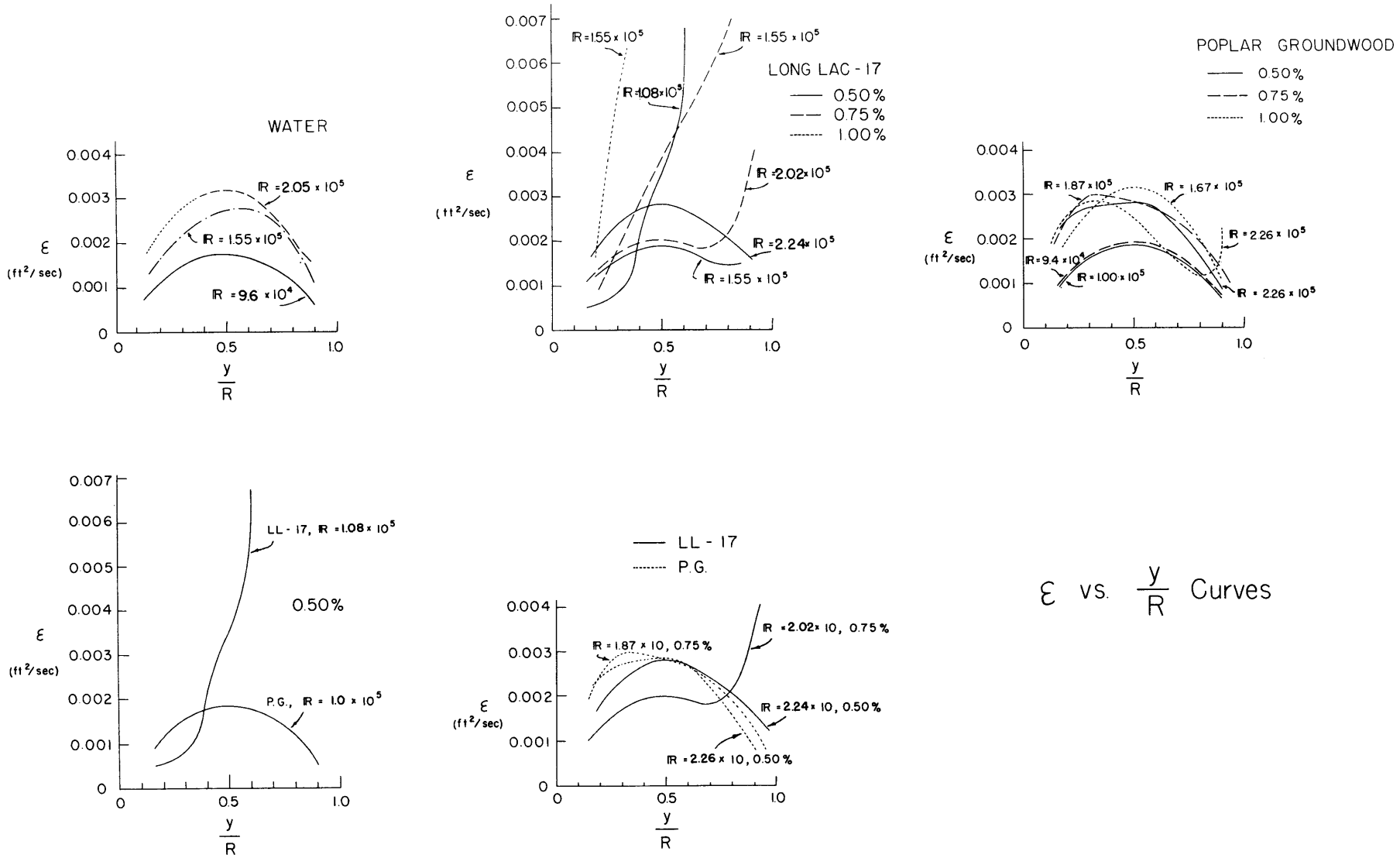

ε vs. $\frac{y}{R}$ Curves

Fig. 18 Overall Momentum Transfer Coefficients ε Computed from Velocity Profiles of Fig. 16

TECHNICAL REPORTS*

Hydrodynamics Laboratory
Department of Civil and Sanitary Engineering
Massachusetts Institute of Technology

NO.	AUTHORS	TITLE	SPONSOR	DATE
1	A.T. Ippen, D.R. Harleman	Studies on the Validity of the Hydraulic Analogy to Supersonic Flow, Parts I and II	U.S. Air Force, USAF TR 5985	May, 1950
2	J.W. Daily, K.C. Deemer, A.L. Keller	The Unsteady Flow Water Tunnel at the Massachusetts Institute of Technology	Office of Naval Research	May, 1951
3	A.T. Ippen, R.S. Yoseph, B.N. Posthill	The Continuous Measurement of Oxygen Concentration in Water during Aeration Processes	U. S. Public Health Service	Mar., 1951
4	A.T. Ippen, D.R. Harleman	Studies on the Validity of the Hydraulic Analogy to Supersonic Flow, Part III	U.S. Air Force, USAF TR 5985	Oct., 1950
5	A.T. Gifford, R.E. Nece, R.E. DuBois	Water Tests of Eight-Inch Check and Stop Valves	U.S. Atomic Energy Commission	Aug., 1953
6	D.R. Harleman, H.E. Crossley	Studies on the Validity of the Hydraulic Analogy to Supersonic Flow, Part IV	U.S. Air Force, USAF TR 5985	Feb., 1952
7	A.T. Ippen, L.G. Campbell, C.E. Carver, Jr.	Determination of Oxygen Absorption in Aeration Processes	U.S. Public Health Service	May, 1952
8	J.W. Daily, S.C. Stephan	The Solitary Wave--Its Celerity, Profile, Internal Velocities and Amplitude Attenuation	Office of Naval Research	July, 1952
9	J.W. Daily, K.C. Deemer	Measurements of Fluid Friction with Steady and Unsteady Motion	Office of Naval Research	July, 1952
10	J.W. Daily, W.L. Hankey	Resistance Coefficients for Accelerated Flow Through Orifices	Office of Naval Research	Oct., 1953
11	H.E. Crossley, D.R. Harleman	Studies on the Validity of the Hydraulic Analogy to Supersonic Flow, Part V - Towed Model Investigation of Transonic Flow	U.S. Air Force, USAF TR 5985	Dec., 1952
12	D.R. Harleman, O.A. Boedtker	Water Table Experiments on Transient Shock Wave Diffraction, Part I, Operation, Instrumentation and Preliminary Experiments	U.S. Air Force	Aug., 1953
13	D.R. Harleman, O.A. Boedtker, S. Wolf	Water Table Experiments on Transient Shock Wave Diffraction, Part II, Experimental Results and Evaluation	U.S. Air Force	Oct., 1954
14	A.T. Ippen, C.E. Carver, Jr.	Oxygen Absorption and Turbulence Characteristics in Bubble Aeration	U.S. Public Health Service	Apr., 1955
15	A.T. Ippen, G. Kulin	Shoaling and Breaking of the Solitary Wave	Office of Naval Research	Apr., 1955
16	A.T. Ippen, G. Kulin, Mir A. Raza	Damping Characteristics of the Solitary Wave	Office of Naval Research	Apr., 1955
17	D.R. Harleman, R.S. Gooch, A.A. Vulgaropulos	Hydraulic Model Performance of Spillway and Outlet Works of Peligre Dam	Brown and Root, Inc.	Apr., 1955
18	A.T. Ippen, P.S. Eagleson	A Study of Sediment Sorting by Waves Shoaling on a Plane Beach	Beach Erosion Board	May, 1955
19	D.R. Harleman, W.C. Shapiro	Experimental and Analytical Studies of Wave Forces on Basic Components of Offshore Structures, Part I: Results for Vertical Cylinders	Humble Oil Company	May, 1955
20	A.T. Ippen, R.S. Tankin, F. Raichlen	Turbulence Measurements in Free Surface Flow with an Impact Tube-Pressure Transducer Combination	Office of Naval Research and the David Taylor Model Basin	July, 1955
21	J.W. Daily, V.E. Johnson	Turbulence and Boundary Layer Effects on the Inception of Cavitation from Gas Nuclei	Office of Naval Research	July, 1955
22	J.W. Daily, J.M. Jordaan	Effects of Unsteadiness on Resistance and Energy Dissipation	Office of Naval Research	Dec., 1956
23	A.T. Ippen, M.M. Mitchell	The Damping of the Solitary Wave from Boundary Shear Measurements	Office of Naval Research	June, 1957
24	D.R. Harleman, W.C. Shapiro, T.A. Marlow, II	Experimental and Analytical Studies of Wave Forces on Offshore Drilling Structures. Part II: Buoyancy Components for Floating Platforms	Humble Oil Company	June, 1957
25	P.S. Eagleson, T.A. Marlow, C.T. Ike, F.J. Turpin	Hydraulic Model Study of Protective Works for Fleet Berthing Facilities in Coddington Cove, Narragansett Bay, R. I.	First Naval District, Boston, Mass.	June, 1957
26	P.S. Eagleson, R.G. Dean, L.A. Peralta	The Mechanics of the Motion of Discrete Spherical Bottom Sediment Particles Due to Shoaling Waves	Beach Erosion Board	Oct., 1957
27	J.W. Daily, R.E. Nece	Roughness and Chamber Dimension Effects on Induced Flow and Frictional Resistance of Enclosed Rotating Disks	Office of Ordnance Research	May, 1958
28	D.R. Harleman, W.C. Shapiro	Investigation on the Dynamics of Moored Structures in Waves	Humble Oil and Refining Co.	July, 1958
29	F. Ursell, R.G. Dean, Y.S. Yu	Forced Small-Amplitude Water Waves: A Comparison of Theory and Experiment	Office of Naval Research	July, 1958
30	J.W. Daily, G. Bugliarello	The Effects of Fibers on Velocity Distribution, Turbulence and Flow Resistance of Dilute Suspensions	Technical Association of the Pulp and Paper Industry	Oct., 1958
31	D.R. Harleman, J.M. Jordaan, J.D. Lin	Diffusion of Two Fluids of Different Density in a Homogeneous Turbulent Field	Nat.Inst.of Health, Dept. of Health, Educ.and Welfare	Feb., 1959
32	P.S. Eagleson	The Damping of Oscillatory Waves by Laminar Boundary Layers	Beach Erosion Board, U.S.Dept. of the Army, Corps of Engrs.	Apr., 1959
33	D.R. Harleman, R.S. Broughton, C.J. Huval, H.W. Partenscky	Model Study of a Flood Control Pumping Station at the Charles River Dam	Metro.Dist.Commission, Commonwealth of Massachusetts	June, 1959
34	J.W. Daily, J.D. Lin, R.S. Broughton	The Distribution of Mean Static Pressure in Turbulent Boundary Layers in Relation to Inception of Cavitation	Office of Naval Research	June, 1959
35	J.W. Daily, G. Bugliarello, W.W. Troutman	Measurement and Analysis of Turbulent Flow of Wood Pulp Fiber Suspensions	Tech.Assoc.of the Pulp and Paper Industry	Sept.,1959

* Technical Reports and Technical Notes, if available, may be obtained from the Hydrodynamics Laboratory at a charge of $1.50 per copy.

STAFF PUBLICATIONS

Hydrodynamics Laboratory
Department of Civil and Sanitary Engineering
Massachusetts Institute of Technology

NO.	AUTHORS	TITLE	PUBLISHED	DATE
1	A.T. Ippen	The New Hydrodynamics Laboratory	Technology Review, M.I.T.	June, 1951
2	A.T. Ippen, and Staff of Hydrodynamics Laboratory	Hydrodynamics in Modern Technology, A symposium held at the Dedication of the Hydrodynamics Laboratory	Hydrodynamics Laboratory, MIT	Apr., 1952
3	A.T. Ippen	The Influence of Viscosity on Centrifugal Pump Performance	Trans. A.S.M.E.	Nov., 1946
4	J.W. Daily	Cavitation Characteristics and Infinite Aspect Ratio Characteristics of Hydrofoil Section	Trans. A.S.M.E.	Apr., 1949
5	A.T. Ippen	Mechanics of Supercritical Flow, Symposium on High-Velocity Flow in Open Channels	Trans. A.S.C.E., Vol. 116	1951
6	A.T. Ippen, J.W. Dawson	Design of Channel Contractions, Symposium on High-Velocity Flow in Open Channels	Trans. A.S.C.E., Vol. 116	1951
7	A.T. Ippen	Channel Transitions and Controls,	Chapter VIII, Engineering Hydraulics (ed. by H.Rouse), John Wiley and Sons	1950
8	J.W. Daily	Hydraulic Machinery	Chapter XIII, Engineering Hydraulics (ed. by H.Rouse), John Wiley and Sons	1950
9	A.T. Ippen, D.R. Harleman	Steady State Characteristics of Subsurface Flow, Symposium on Gravity Waves	National Bureau of Standards NBS Circular 521	June, 1951
10	A.T. Ippen, D.R. Harleman	Certain Quantitative Results of the Hydraulic Analogy to Supersonic Flow	Proc.,Second Midwestern Conference on Fluid Mechanics, Ohio State University	Mar., 1952
11	H.M. Paynter	Methods and Results from M.I.T. Studies in Unsteady Flow	Jr.,Bos.Soc.of Civil Engrs.	Apr., 1952
12	J.W. Daily, S.C. Stephan	Characteristics of the Solitary Wave	Trans. A.S.C.E., Vol. 118	1953
13	H.M. Paynter	Electrical Analogies and Electrical Computers: Surge and Water Hammer Problems	Trans. A.S.C.E., Vol. 118	1953
14	J.W. Daily, K.C. Deemer	The Unsteady Flow Water Tunnel at the Massachusetts Institute of Technology	Trans. A.S.M.E., Vol. 76, No.1	Jan., 1954
15	A.T. Ippen, C.E. Carver	Continuous Measurement of Dissolved Oxygen with Dropping Mercury and Rotating Platinum Electrodes, Conference on Instrumentation in Water, Sewage and Industrial Waste Treatment, Manhattan College, May, 1953.	Insturments and Automation, Vol. 27	Jan., 1954
16	A.T. Ippen, R.P. Verma	The Motion of Discrete Particles Along the Bed of a Turbulent Stream	Proc.,Minn.International Hydraulics Convention Trans. A.S.C.E.	1955
17	J.W. Daily, S.C. Stephan	The Solitary Wave -- Its Celerity, Profile, Internal Velocities and Amplitude Attentuation in a Horizontal Smooth Channel	Proc., Third Conference on Coastal Engineering, Cambridge, Massachusetts	Oct., 1952
18	A.T. Ippen, D.R. Harleman	Maintenance of a Navigable Channel through a Breakthrough Area	Proc., Fourth Conference on Coastal Engineering, Chicago, Illinois	Oct., 1953
19	A.T. Ippen, C.E. Carver	Basic Factors of Oxygen Transfer in Aeration Systems	Sewage and Industrial Wastes, Vol. 26, No. 7	July, 1954
20	D.R.Harleman, A.T. Ippen	The Range of Application of the Hydraulic Analogy in Transonic and Supersonic Aerodynamics	Anniversary Volume for M.D. Riabouchinsky, Pub. Scientifiques et Tech. du Ministere de l'Air, Paris, France	May, 1954
21	A.T. Ippen, D.R. Harleman	Verification of Theory for Oblique Standing Waves, A.S.C.E. Proc. Separate No. 526, Vol. 80, Oct., 1954	Trans., A.S.C.E.	1956
22	J.W. Daily, A.T. Ippen	Some Instruments and Facilities of the M.I.T. Hydrodynamics Laboratory	Proc., Joint Admiralty and U.S. Navy Meeting on Hydroballistics, Teddington, England	Sept., 1954
23	D.R. Harleman	Effect of Baffle Piers on Stilling Basin Performance	Jr. Bos.Soc.of Civil Engrs.	Apr., 1955
24	A.T. Ippen, G. Kulin	The Shoaling and Breaking of the Solitary Wave	Proc., Fifth Conference on Coastal Engineering, Grenoble, France	Sept., 1954
25	R.E. Nece, R.E. DuBois	Hydraulic Performance of Check and Control Valves	Jr. Bos.Soc.of Civil Engrs.	July, 1955
26	C.R. Carver	Absorbtion of Oxygen in Bubble Aeration	Proc., Biological Treatment of Sewage and Industrial Wastes Conference, Manhattan College, N.Y., Reinhold Publ. Corp., N.Y.	Apr., 1955
27	A.T. Ippen, P.S. Eagleson	A Study of Sediment Sorting by Waves Shoaling on a Plane Beach	Proc., I.A.H.R. Meeting, Delft, Netherlands	Sept., 1955
28	J.W. Daily, W.L. Hankey, R.W. Olive, J.M. Jordaan	Resistance Coefficients for Accelerated and Decelerated Flows through Smooth Tubes and Orifices	Trans. A.S.M.E.	July, 1956
29	A.T. Ippen	Hydrodynamic Models of Pressure Conduits	Proc., International Congress on Models in Technology, Venice	Oct., 1955
30	J.W. Daily, V.E. Johnson	Turbulence and Boundary Layer Effects on Cavitation Inception from Gas Nuclei	Proc., Symposium on Cavitation in Hydrodynamics, National Physical Laboratory, Teddington, England	Sept., 1955
31	A.T. Ippen, P.S. Eagleson	A Study of Sediment Sorting by Waves Shoaling on a Plane Beach	Beach Erosion Board Tech. Memorandum No. 63	Sept., 1955

STAFF PUBLICATIONS
(Contd)

NO.	AUTHORS	TITLE	PUBLISHED	DATE
32	G.R. Williams	Hydrology	Chapter IV of Engineering Hydraulics (edited by H.Rouse), John Wiley and Sons	1950
33	J.M. Jordaan	Some Aspects of the Design and Stability Analysis of Spillways on Alluvium	Trans., South African Inst.of Civil Engineers, Vol.6, No.2	Feb., 1956
34	A.T. Ippen	Hydrodynamics: A Review of von Karman's Contributions	Special Issue of the Journal of Aeronautical Sciences in honor of Th. von Karman	May, 1956
35	J.W. Daily, V.E. Johnson	Turbulence and Boundary Layer Effects on Cavitation Inception from Gas Nuclei	Trans, A.S.M.E., Vol.78, No.8	Nov., 1956
36	A.T. Ippen, G. Kulin	The Effect of Boundary Resistance on Solitary Waves, (L'effet produit sur les ondes solitaires par le frottement a la paroi)	La Houille Blanche, No.3	July, Aug., 1957
37	J.G. Housely, D.C. Taylor	Application of the Solitary Wave Theory to Shoaling Oscillatory Waves	Trans. Amer.Geophys.Union	Feb., 1957
38	P.S. Eagleson	Properties of Shoaling Waves by Theory and Experiment	Trans., Amer.Geophysical Union	Oct., 1956
39	D.R. Harleman, R.S. Gooch, A.T. Ippen	Submerged Sluice Gate Control of Density Currents	Proc. A.S.C.E. Hydr.Division	Apr., 1958
40	A.T. Ippen, F. Raichlen	Turbulence in Civil Engineering Measurements in Free Surface Streams (with an Impact Tube-Pressure Cell Combination)	Symposium on Turbulence in Civil Engineering, Proc. A.S.C.E., Hydro.Division	Oct., 1957
41	A.T. Ippen, J.W. Daily, G. Bugliarello	Pertinent Factors in Flow Research on Dilute Fiber Suspensions	TAPPI Mag. Vol.40, No.6	June, 1957
42	D.R. Harleman	Density Currents Studied in Glass-Walled Flume	Civil Engineering,	Feb., 1954
43	P.S. Eagleson	Hydraulic Model Study of Protective Works for Fleet Berths in Narragansett Bay	Trans. Bos.Soc.of Civil Engrs, Vol.46, No.1	Jan., 1959
44	P.S. Eagleson, L.A. Peralta, R.G. Dean	Motion of Discrete Bottom Sediment Particles due to Shoaling Waves	Beach Erosion Board, Tech. Memorandum #104	Feb., 1958
45	J.W. Daily, R.E. Nece	Chamber Dimension Effects on Induced Flow and Frictional Resistance of Enclosed Rotating Disks	A.S.M.E. Paper No.59-Hyd-9	Apr., 1959
46	D.R. Harleman	Discussion on Turbulent Characteristics of the Hydraulic Jump, by Hunter Rouse, et al.,(A.S.C.E., Proc. Paper 1528, February, 1958)	Jr. of Hydraulics Division, A.S.C.E.	Nov., 1958

TECHNICAL NOTES*

NO.	AUTHORS	TITLE	SPONSOR	DATE
1	R.E. Nece	Water Test Results for an Experimental "Ten-Inch" Swing Check Valve	Westinghouse Electric Corp.	July, 1956
2	J.W. Daily, G. Bugliarello	The Characteristics of Flow with Dilute Fiber Suspensions. A Progress Report of Work under TAPPI Project 93	Tech.Assoc.of the Pulp and Paper Industry	Dec., 1957
3	G.H. Toebes, F.E. Perkins, P.S. Eagleson	Design of a Closed Jet, Open Circuit Water Tunnel for the Study of Wake Mechanics	David Taylor Model Basin	Apr., 1958
4	J.W. Daily, A. Tsuchiya	Flow of Nylon Fiber Suspensions. A Progress Report on a Phase of Work under TAPPI Project 147	Tech.Assoc.of the Pulp and Paper Industry	Feb., 1959
5	F.E. Perkins, P.S. Eagleson	The Development of a Total Head Tube for High Frequency Pressure Fluctuations in Water	David Taylor Model Basin	July, 1959
6	R.E. Nece, C.A. Givler	Measurement of Boundary Shear Stresses in an Open Channel Curve with a Surface Pitot Tube	ARS, U.S. Dept.of Agriculture	Aug., 1959

* Technical Reports and Technical Notes, if available, may be obtained from the Hydrodynamics Laboratory at a charge of $1.50 per copy.